UNIVERSITA' DEGLI STUDI

DI MODENA E REGGIO EMILIA

International Doctorate School in Clinical and Experimental Medicine (CEM)

Cycle XXXVI

AUTOFLUORESCENCE AS A POTENTIAL DIAGNOSTIC TOOL FOR THE DETECTION OF SKIN TUMORS:

FROM EX- VIVO TO IN VITRO EVALUATION

Candidate: Dr. Federico Garbarino

Tutor: Prof.ssa Cristina Magnoni

Co-tutor: Prof. Giovanni Pellacani

PhD Program Coordinator: Prof. Marco Vinceti

Abstract:

Autofluorescence (AF) is the emission of light observed in certain tissues, linked to the presence and arrangement of specific molecules known as fluorophores, which have the ability to absorb and then re-emit light at particular wavelengths. In dysplastic and malignant lesions, both cells and extracellular components may exhibit changes in the quantity, distribution, and physical-chemical properties of these intrinsic fluorophores. Biological tissues can absorb and subsequently re-emit light of specific wavelengths, which can be detected using spectrophotometric devices.

Melanoma and Non-Melanoma Skin Cancer (NMSC) are among the most common neoplasms worldwide, particularly prevalent in individuals with fair skin. The objective of our research was to investigate the effectiveness of AF in distinguishing between healthy and cancerous tissues, spanning from ex-vivo to in vitro evaluations. The studies that were carried out in this setting are the following:

-A pre-clinical ex vivo study was performed in order to investigate the relationship between the intensity of cutaneous autofluorescence (AF) and the histopathological characteristics of malignant and pre-malignant skin lesions, focusing on Non-Melanoma Skin Cancers (NMSCs). An experimental spectrophotometric system was developed to quantitatively and objectively assess the fluorescence intensity.

The fluorescence intensity was compared with different histopathological variables (diagnosis, hyperkeratosis, epithelial thickening, fibrosis, elastosis, neovascularization and cellular atypia) in order to identify which were the most relevant features in influencing the fluorescence pattern of the lesion.

- A second investigation was conducted to compare the in vitro autofluorescence (AF) emission spectra of squamous carcinoma cells and healthy control cells. SCC154 cells and healthy keratinocytes obtained from pools of donors were used for this purpose. The choice of working on cells rather than tissues was aimed at identifying specific

intrinsic autofluorescence characteristics of cancer possibly responsible for AF variations. In addition to AF spectra within the visible spectrum, absorption measurements were also performed.

Interestingly, markedly distinctive emission and absorption patterns were detected for healthy control cells and pathological cells, due to differences in endogenous chromophores such as FAD, NAD(P)H, lipo-pigments, and porphyrins.

-Another comparative in-vitro autofluorescence study was then performed on skin-derived cell lines (either healthy or tumoral) in order to exclude previous results possibly being biased by the heterogeneity of cell sources.

Comparative analysis of the autofluorescence from squamous carcinoma cells and healthy human keratinocytes derived from cell lines confirmed distinctive AF characteristics, with control cells exhibiting clear emission patterns associated with typical endogenous chromophores.

Our research stresses the importance of autofluorescence (AF) as a potential tool for the detection of skin tumors. Through in vitro assessments, we have demonstrated that AF alterations are detectable both at a cell and at a tissue level in cutaneous neoplasms.

Abstract in italiano:

L'autofluorescenza (AF) è l'emissione di luce osservata in certi tessuti, legata alla presenza e all'organizzazione di specifiche molecole chiamate fluorofori, che hanno la capacità di assorbire e poi riemettere luce a lunghezze d'onda particolari. In lesioni displastiche e maligne, sia le cellule che i componenti extracellulari possono mostrare cambiamenti nella quantità, distribuzione e proprietà fisico-chimiche di questi fluorofori intrinseci. I tessuti biologici possono assorbire e successivamente riemettere luce con specifiche lunghezze d'onda, che può essere rilevate mediante dispositivi spettrofotometrici.

Il melanoma e il cancro della pelle non melanoma (NMSC) sono tra le neoplasie più comuni al mondo, particolarmente diffuse nelle persone con pelle chiara. L'obiettivo della nostra ricerca era investigare l'efficacia dell'AF nel distinguere tra tessuti sani e cancerogeni, spaziando dalle valutazioni ex-vivo a quelle in vitro. Gli studi condotti in questo contesto sono i seguenti:

È stato effettuato uno studio ex vivo preclinico al fine di investigare la relazione tra l'intensità dell'autofluorescenza cutanea (AF) e le caratteristiche istopatologiche di lesioni cutanee maligne e premaligne, concentrandosi sui tumori della pelle non melanoma (NMSC). È stato sviluppato un sistema spettrofotometrico sperimentale per valutare quantitativamente e oggettivamente l'intensità della fluorescenza. L'intensità della fluorescenza è stata confrontata con diverse variabili istopatologiche (diagnosi, ipercheratosi, ispessimento epiteliale, fibrosi, elastosi, neovascolarizzazione e atipia cellulare) al fine di identificare le caratteristiche più rilevanti che influenzavano il modello di fluorescenza della lesione.

Un secondo studio è stato condotto per confrontare gli spettri di emissione dell'autofluorescenza (AF) in vitro delle cellule di carcinoma squamoso e delle cellule di controllo sane. Le cellule SCC154 e i cheratinociti sani ottenuti da gruppi di donatori sono stati utilizzati a questo scopo. La scelta di lavorare sulle cellule piuttosto che sui

tessuti mirava a identificare specifiche caratteristiche intrinseche dell'autofluorescenza del cancro responsabili delle variazioni dell'AF. Oltre agli spettri di AF nel campo visibile, sono state eseguite anche misurazioni di assorbimento.

In modo interessante, sono stati rilevati schemi di emissione e assorbimento marcatamente distintivi per le cellule di controllo sane e le cellule patologiche, a causa delle differenze nei cromofori endogeni come FAD, NAD(P)H, lipopigmenti e porfirine.

Un altro studio comparativo in vitro sull'autofluorescenza è stato quindi condotto su linee cellulari derivate dalla pelle (sane o tumorali) al fine di escludere che i risultati precedenti fossero possibilmente influenzati dall'eterogeneità delle fonti cellulari.

L'analisi comparativa dell'autofluorescenza delle cellule di carcinoma squamoso e dei cheratinociti umani sani derivati da linee cellulari ha confermato caratteristiche distintive dell'AF, con le cellule di controllo che mostravano chiari schemi di emissione associati a cromofori endogeni tipici.

La nostra ricerca sottolinea l'importanza dell'autofluorescenza (AF) come potenziale strumento per la rilevazione di tumori della pelle. Attraverso valutazioni in vitro, abbiamo dimostrato che le alterazioni dell'AF sono rilevabili sia a livello cellulare che a livello di tessuto nelle neoplasie cutanee.

1 Physical and biological bases of fluorescence

1.1 Phenomena of fluorescence

Luminescence refers to the emission of light from a substance when it is in an electronically excited state. This phenomenon is formally categorized into two main types: fluorescence and phosphorescence, depending on the nature of the excited state.

Historically, the differentiation between fluorescence and phosphorescence was primarily based on the duration of light emission following excitation. Fluorescence was defined as the emission of light that ceased simultaneously with the end of excitation, while phosphorescence was characterized by emitted light persisting after the excitation had ended[1]. However, this distinction became inadequate over time, as there are instances of long-lived fluorescence (e.g., divalent europium salts) and short-lived phosphorescence (e.g., the violet luminescence of zinc sulfide) with comparable durations, typically in the range of several hundreds of nanoseconds.

To more accurately describe these phenomena in the context of molecular photochemistry, it is now understood that fluorescence retains the same spin multiplicity as the excited state, whereas phosphorescence involves a change in spin multiplicity, often transitioning from triplet to singlet or vice versa. (Figure 1)[2]

One notable characteristic of fluorescence is its high sensitivity in detection. As far back as 1877, fluorescence sensitivity was employed to demonstrate the connection between the Danube and Rhine rivers through underground streams. In this demonstration, 10 kg of fluorescein dye was introduced into the Danube, and about sixty hours later, its distinctive green fluorescence was observed in a small river leading to the Rhine. In modern times, fluorescence tracing is widely utilized in

hydrogeology, particularly for simulating and tracking the movement of pollutants in groundwater systems.

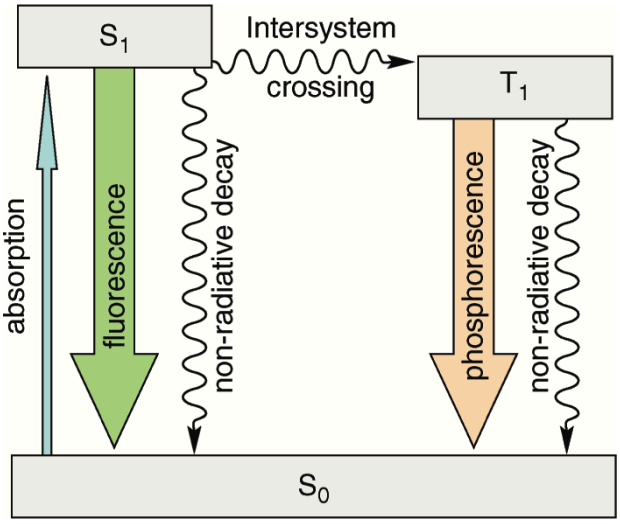

Figure 1. Simplified Perrin Jablonski diagram showing the difference between fluorescence and phosphorescence.

Fluorescence takes place when radiation is emitted from the initial excited singlet state, denoted as S1, which is achieved through the absorption of a photon beforehand. In contrast, phosphorescence occurs when radiation is emitted from the triplet state, known as T1, following intersystem crossing from S1.

1.2 History of fluorescence

In 1565, a Spanish physician and botanist named Nicolás Monardes published the "Historia medicinal de las cosas que se traen de nuestras Indias Occidentales," wherein he described an interesting phenomenon: the bluish opalescence observed in a water infusion derived from the wood of a small Mexican tree. This particular wood, later referred to as "Lignum nephriticum," exhibited unique color properties and possessed diuretic qualities. Even in the time of the Aztecs, this wood was recognized as a rare and costly medicinal substance. Monardes' discovery can be considered one of the earliest recorded observations of what would later be termed "fluorescence."

Subsequently, extracts from this wood were further explored by prominent scientists like Boyle, Newton, and others, although the underlying phenomenon remained a mystery during that era. It was only recently that the chemical species responsible for the intense blue fluorescence observed in an infusion of L. nephriticum (E. polystachya) was identified, known as "matlaline" derived from the Aztec word "Matlali" meaning blue. Interestingly, matlaline does not naturally exist in the plant; rather, it results from an unusual spontaneous oxidation of at least one of the tree's flavonoids.[2]

In 1664, Robert Boyle, inspired by Monardes' findings, conducted further investigations into this system. He noted that after multiple infusions, the wood lost its ability to impart color to the water and concluded that there must be some "essential salt" within the wood responsible for this effect. Boyle also discovered that the addition of acid eliminated the color, while the addition of alkali restored it.

Fast forward to 1819, a remarkable property of certain fluorite crystals (calcium fluoride, then known as "fluated lime," "spath fluor," or "fluor spar") from Weardale, Durham, England, was documented by Edward D. Clarke, a Professor of Mineralogy at the University of Cambridge.[3]

In 1833, the renowned Scottish physicist David Brewster described the exquisite red fluorescence of chlorophyll in his article "On the Color of Natural Bodies." He noted that when a beam of sunlight passed through a green alcoholic extract of leaves (primarily a chlorophyll solution), it appeared red when observed from the side. He drew a parallel between this phenomenon and the blue light emitted when a light beam entered certain fluorite crystals.[4]

In 1845, John Herschel (Figure 2) made a significant observation of fluorescence from quinine sulfate and termed this phenomenon "epipolic dispersion." He created an acid solution of quinine sulfate and documented his findings.

1.3 The origin of the word “fluorescence”

Sir George Gabriel Stokes, a physicist and mathematics professor at Cambridge University, in 1852 published his renowned paper titled "On the Refrangibility of Light."[1] In this paper, he conducted comprehensive experimental investigations on various substances, encompassing both organic (such as quinine) and inorganic (like fluorite crystals). He identified a common phenomenon that he termed "dispersive reflection," where the wavelengths of the scattered light were consistently longer than those of the original incident light.[2]

Stokes employed a prism to disperse the solar spectrum and directed it onto a solution of quinine. He observed that no discernible effect occurred until the solution was exposed to the ultraviolet portion of the spectrum. This observation led Stokes to assert that fluorescence emitted light of longer wavelength than the exciting light, which ultimately resulted in this spectral shift being named the "Stokes Shift." In his own words, he remarked, "I confess that I do not like this term. I am almost inclined to create a new word, calling the phenomenon 'fluorescence,' inspired by the term 'fluor-spar,' similar to how the word 'opalescence' is derived from a mineral name."

However, it is noteworthy that a decade before Stokes's groundbreaking paper, the French physicist Edmond Becquerel had published an original work in which he described the emission of light when calcium sulfide was deposited on paper and exposed to solar light, particularly beyond the violet part of the spectrum. Becquerel was, therefore, the first to assert that the emitted light had a longer wavelength than the incident light. Stokes's paper led to a claim by Becquerel for priority in this

discovery. It's worth noting that, as per the definitions provided earlier, quinine exhibits fluorescence, while calcium sulfide demonstrates phosphorescence, although both phenomena fall under the umbrella of photoluminescence[3].

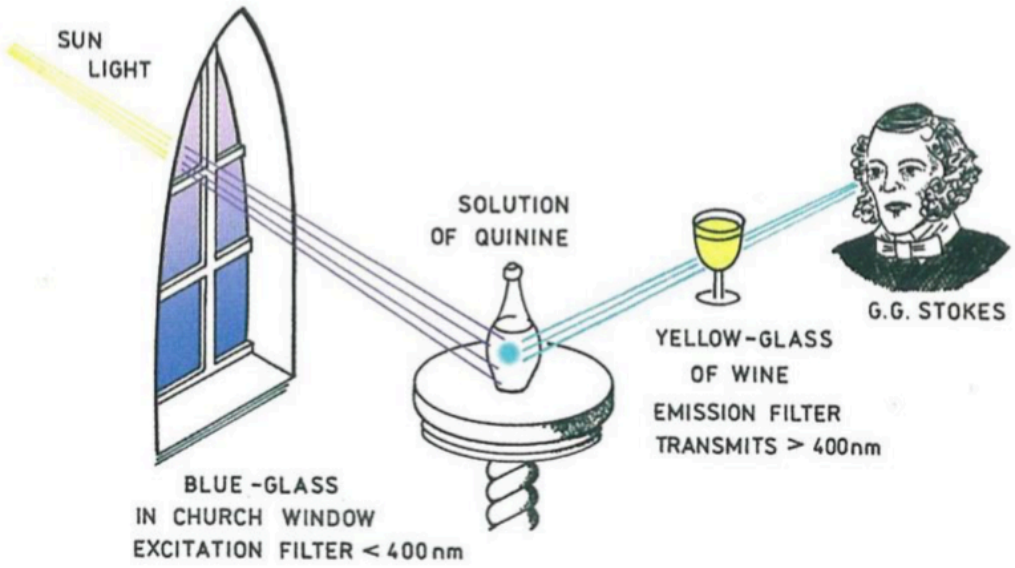

Figure 2. Experimental set-up used by GG Stokes (Lakowicz, 1999).

1.4 Jablonski diagram

Aleksander Jablonski was a dedicated Polish scholar who devoted his life to researching the absorption and emission of light by molecules. He developed a visual representation known as the Jablonski diagram, which provides an overview of the possible outcomes when photons from the visible spectrum interact with a molecule. Figure three illustrates a typical Jablonski diagram, featuring the singlet ground state (S0) and the first (S1) and second (S2) electronic states. Each electronic energy level can have various vibrational energy levels represented as 0, 1, 2, and so forth.

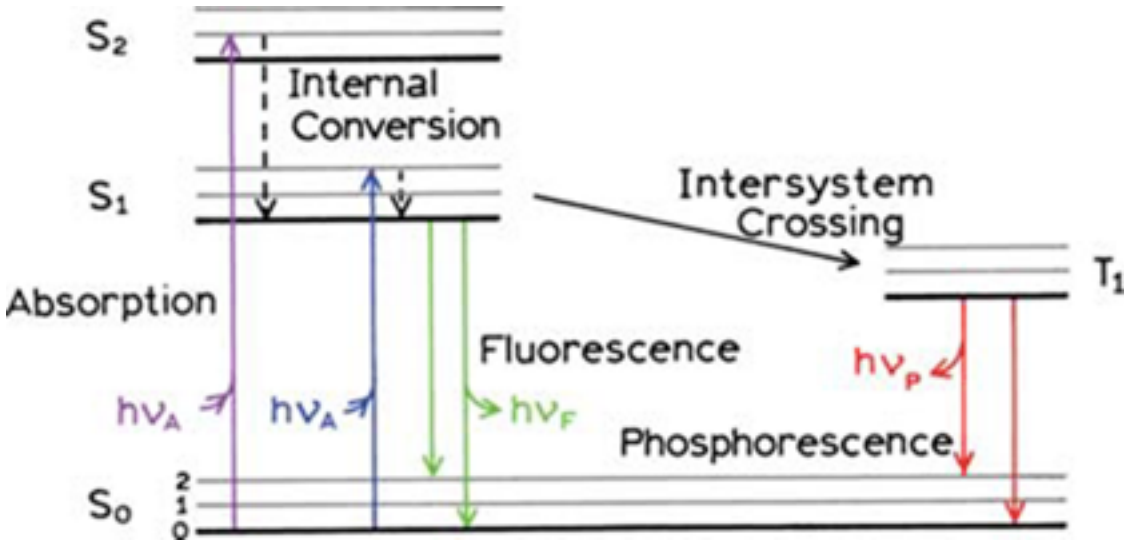

Figure 3. Jablonski diagram (adapted from J. R. Lakowicz, Principles of Fluorescence Spectroscopy, 3rd Ed., Springer, 2006)

Transitions between these states are depicted as vertical lines, and these transitions typically occur in a remarkably short time, around 10^{-15} seconds, which is too brief for significant displacement of atomic nuclei. This phenomenon aligns with the Franck-Condon principle.[5]

After absorbing light, several typical processes ensue. Usually, a fluorophore is excited to a higher vibrational level in either S1 or S2. In most cases, molecules in condensed phases rapidly relax to the lowest vibrational level of S1, a process referred to as internal conversion. This internal conversion generally occurs within 10^{-12} seconds or less. Since fluorescence lifetimes are typically around 10^{-8} seconds, internal conversion is usually completed before emission. Consequently, fluorescence emission primarily results from a thermally equilibrated excited state, specifically the lowest energy vibrational state of S1. Molecules in the S1 state can also undergo a spin conversion to the first triplet state, T1, leading to phosphorescence emission. Phosphorescence emissions generally occur at longer wavelengths (lower energy) compared to fluorescence due to the conversion from S1 to T1, a process known as intersystem crossing. Transition from T1 to the singlet ground state is prohibited,

resulting in rate constants for triplet emission several orders of magnitude smaller than those for fluorescence.[1,5]

Excitation and emission spectra are fundamental for characterizing fluorescent molecules. The excitation spectrum demonstrates the likelihood of exciting a fluorescent molecule with different wavelengths of incident light while keeping the emission wavelength constant. In essence, the excitation spectrum is similar to the absorption spectrum when excitation intensity remains constant. The maximum of the excitation peak corresponds to the energy difference between the ground state (S0) and a favored vibrational level of the first excited state (S1)

Some cases may exhibit a second peak at a shorter wavelength (higher energy) indicating the transition of the molecule from the ground state to the second excited state (S2). (Figure 4)[6]

.

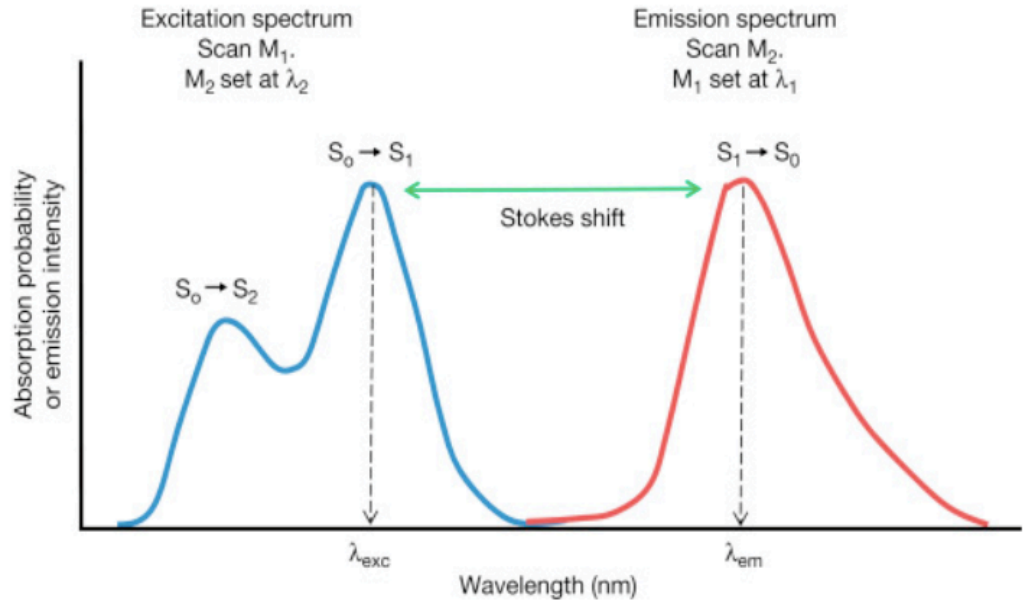

7

Figure 4. Features of excitation and emission fluorescence spectra

On the other hand, the fluorescence emission spectrum is a plot of the relative intensity of emitted light as a function of emission wavelength at a fixed excitation wavelength. The shape of the emission spectrum mirrors the lowest wavelength excitation band and is always shifted towards longer wavelengths relative to the excitation spectrum. This difference between the excitation and emission maxima is termed the "Stokes shift," representing the energy lost while the molecule was in the excited state. The Stokes shift facilitates the separation and distinction of excitation and emission peaks.

The emission wavelength and fluorescence intensity depend on the molecule's structure. While theoretically, any molecule absorbing adequate energy could fluoresce, many exhibit weak fluorescence, and only a fraction is analytically useful. To quantify fluorescence capability, the concept of fluorescence quantum yield is introduced, defined as the fraction of emitted photons per absorbed photon. Determining this quantum yield can be done either absolutely, using an integrating sphere, or relatively, employing fluorescence standards. Although the thesis did not determine the fluorescence quantum yield, the emission intensities can be compared, as all emission spectra were acquired using a consistent setup with a fixed excitation intensity, consistent illumination, and fixed collection parameters.

1.5 Fluorophores of the skin

Fluorophores are the molecules able to absorb and reemit light of specific wavelength. (Figure. 5)

They are conventionally divided into two main classes, intrinsic and extrinsic. The intrinsic are present naturally in the human tissue, extrinsic are those added to a sample that hasn't got specified spectral properties.

The relationship of many endogenous fluorophores with morpho-functional properties of the living systems, which are influencing their AF emission features, affords the powerful resource for monitoring the biological substrate condition.

Molecules identified as possible fluorophores in the skin were porphyrins, advanced glycation end products (AGEs), flavins, lipopigment, adenine dinucleotide (NADH), flavin adenine dinucleotide (FAD), pheomelanin, eumelanin, collagen, elastin, tryptophan, components of lipofuscin and keratin.

NAD(P)H and Flavins, coenzymes of key enzymes in redox reactions, represent the main responsible for the AF signal rising from the cytoplasm of the cells.

They absorb light at 330-450nm and re-emit at 440-540nm. AF changes are due to the aerobic/anaerobic metabolism depending on inflammation, carcinogenesis, and antioxidant defense.

Particularly, NADH is more fluorescent than the oxidized form, NAD+[8]. Depending on the metabolic status of cells (e.g., prevalence of reactions of oxidation or reduction), the oxidized or reduced form of the coenzyme will be prevalent in the cytoplasm, thus leading to a higher or lower degree of fluorescence[9]. It has been widely demonstrated that neoplastic cells display an increase in oxidative processes, and it is therefore reasonable to hypothesize a shift in the NAD+/NADH equilibrium toward a predominance of NAD+.[10,11]

Such a low value of the bound/free ratio is, most probably, one of the biological features associated to the loss of AF observed in tumor cells.

Belonging to the category of flavin-free derivatives, FAD demonstrates absorption/excitation and emission characteristics within the 440–450 nm and 525 nm range, respectively. The fluorescence emitted by FAD is notably influenced by the inherent characteristics of the protein to which the prosthetic group is attached.

Porphyrins are indicated as fluorophores in skin tissues, with an excitation wavelength of about 400 nm and emission wavelength around 630–690 nm. Variation in porphyrin concentration is considered an important marker for differentiating malignant disorders from healthy tissues[12].

Delta-aminolevulinic acid (ALA) is one of the most commonly used exogenous compounds for photodynamic diagnostics and therapy, which provides the fluorescence effect. Its local use results in selective accumulation of Protoporphyrin IX (PpIX) in NMSC cells.

Elastin and collagen are the main molecules of the extracellular matrix, which is the great majority structure of the skin tissue. Cancerous tissue is characterized by a disarrangement of the skin extracellular architecture, with reduced content of elastin and collagen, the strongest natural fluorophores. These phenomena result in qualitative and quantitative differences in the spectrum of emitted light of healthy tissues and cancerous tissues[13].

Melanine in the skin tissue demonstrates a very weak of fluorescence. Investigation of melanin fluorescence, within a different set of pigmented lesions of the skin, showed a marked difference in AF behavior of benign pigmentations (e.g.,melanocytic nevi) with respect to melanoma[14].

Finally, it is important to remember that DNA is weakly of fluorescent, in fact it doesn’t participate to the nuclear AF emission, even the membranes typically do not display intrinsic fluorescence.

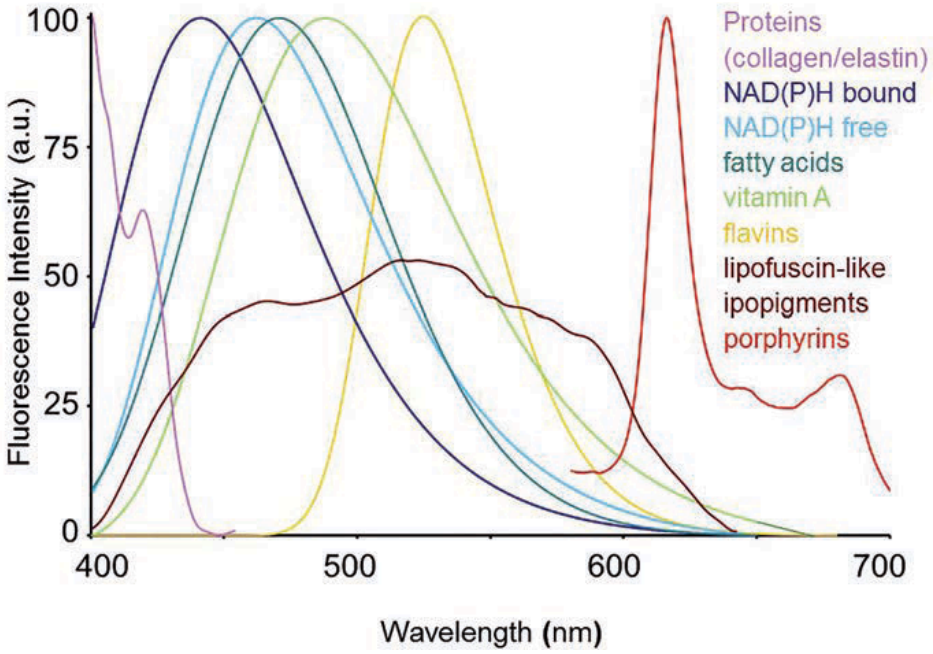

Endogenous fluorophores	Biological constituents	Autofluorescence (exc) / (em) ranges	Autofluorescence photophysical fingerprints and possible correlated alterations
Aromatic amino acids: Phe, Tyr, Trp	Functional proteins	(240-280 nm) / (280-350 nm)	Spectral shape and amplitude (near UV, blue region tail)
Cytokeratins	Intracellular fibrous proteins	(280-325 nm) / (495-525 nm)	Spectral shape and emission amplitude
Collagen/Elastin	Extracellular fibrous proteins	(330-340 nm) / (400-410 nm) (350-420 nm) / (420-510 nm)	Excitation light birifrangence effects spectral shape and emission amplitude, depending on maturation degree in eldering and fibrosis
NAD(P)H	Coenzymes of key enzymes in redox reactions	(330-380 nm) / (440, 462 nm, bound, free)	Spectral shape, emission amplitude
Flavins	Coenzymes of key enzymes in redox reactions	(350-370;440-450 nm) / (480/540 nm)	$(NAD(P)H_{bound/free}$, $NAD(P)H_{total}/_{oxidized}$ $_{flavins}$ ratios, depending on aerobic/anaerobic energetic metabolism, antioxidant defense, inflammation, carcinogenesis
Fatty acids	Accumulated lipids	(330-350 nm) / (470-480 nm)	Spectral shape, emission amplitude and photosensitivity, depending on altered lipid metabolism
Vitamin A	Retinols and carotenoids	(370-380 nm) / (490-510 nm)	Spectral shape, emission amplitude and photosensitivity, depending on multiple functions including antioxidant and vision roles, and altered retinol metabolism
Protoporpyrin IX and porphyrin derivatives	Protein prostetic group	(405 nm) / (630-700 nm)	Spectral shape, emission amplitude and photosensitivity, depending on heme and iron altered metabolism
Lipofuscins/ Lipofuscin like-lipopigments/ceroids	Miscellaneous (proteins, lipids, retinoids)	(UV, 400-500 nm) / (480-700 nm)	Spectral shape, emission amplitude depending on eldering, oxidation degree, cell stemness degree

Figure 5. At the top, typical spectral profiles of autofluorescence emission from single endogenous fluorophores. Spectra were normalized to the maximum emission peak for presentation, except for the broad emission of lipopigments. At the bottom, endogenous fluorophores with different excitation and emission spectra. (Croce, A., & Bottiroli, G. "Autofluorescence spectroscopy and imaging: a tool for biomedical research and diagnosis". European Journal of Histochemistry, 58(4), 2461.)

2 Skin Cancer

Skin cancer incidence increased worldwide, and it is becoming a major public health concern.

This large group of tumors can be divided into three most frequent neoplasms, basal cell carcinoma (BCC) squamous cell carcinoma (SCC) and melanoma.

BCC and SCC can be collected in the Non-Melanoma skin cancer (NMSC) group.

Ultraviolet radiation, genetic predisposition, tobacco, X-ray radiation, nevus count are the main risk factors[15].

2.1 Basal cell carcinoma

BCC is considered the most frequent skin malignancy and the most frequent NMSC. It originates from the basal cell layer of the epidermis.

It can often be aggressive locally, with rare metastatic behavior, with high morbidity.

It is very common in fairy skin people and much less common in darker skin type.

A history of sunburn during childhood seems to be the most important risk factor.

Another strong evidence of the role of the UV exposure in the development of this tumor is represented by the tanning beds and the phototherapy.

UVA treatments (PUVA) appears to be more carcinogenic than UVB light.

Nevoid Basal cell Carcinoma Syndrome due to the PTCH1 mutation is one of the genetic syndromes which predisposes the arising of multiple BCC in young people.

We can recognize many clinical and histological types of BCC, the most common are the nodular, superficial, and infiltrative ones.

Nodular is shiny, pearly papule or nodule with smooth surface, arborising vessels, arising mostly in head and neck regions.

Superficial is an erythematous plaque with rolled borders mainly affecting the trunk of photodamage skin people[16,17,18].

Infiltrative is an ill-defined, flat, indurated plaque, with pink color with an overlying crust, ulceration.

2.2 Squamous cell carcinoma

Squamous cell carcinoma is the malignant neoplasm arising from the spinous layer of the epidermis.

It is the second most common skin neoplasm after BCC. Unlike this one, SCC sometimes has a metastatic behavior, with increased mortality risk, especially when arising inhead and neck skin[19].

Clinically, it appears as an ulcerated and crust nodule, plaque, ulcer, depending on tumor stage.

SCC affecting more frequently elderly people with immunosuppression, history of radiation therapy, sun damage skin, human Papillomavirus infection, chronic inflammation and cigarette smoking for the one arising from lips.

We can subdivide the skin SCC from the histopathological point of view in SCC in situ or Bowen disease, keratoacanthoma, verrucous carcinoma, clear cell carcinoma, spindle cells and adenosquamous carcinoma[15].

This classification depends on the keratinocyte atypia, the extension of this, the differentiation, and the invasiveness in the deeper layer.[20]

2.3 Management

In every type of NMSC surgical treatment is the gold standard.

Punch or shave biopsy are essential as first step for histological diagnose, in BCC and SCC. In some cases when the tumor is classified as Bowen disease or superficial BCC, cryotherapy or Imiquimod are useful treatment options.[21,22,20]

In the great majority of cases, surgical treatment with clear margins, is the best treatment option.[23]

In pigmented lesions as melanoma, margins are very demarcated, in NMSC surgery could be a little bit more complicated with more incidence of positive margins and the need of recut.

Mohs Micrographic surgery is the best treatment option in case of infiltrative tumors, with unclear clinical/dermoscopic margins, in particular for the head and neck region.[24]

3 Correlation between Autofluorescence Intensity and Histopathological Features in Non-Melanoma Skin Cancer: An Ex Vivo Study

3.1 Background

Non-melanoma skin cancer (NMSC) is the most common malignant tumor affecting fair-skinned people. Increasing incidence rates of NMSC have been reported worldwide, which is an important challenge in terms of public health management. Surgical excision with pre-operatively identified margins is one of the most common and effective treatment strategies. Incomplete tumor removal is associated with a very high risk of recurrence and re-excision. Biological tissues can absorb and re-emit specific light wavelengths, detectable through spectrophotometric devices. Such a phenomenon is known as autofluorescence (AF). AF spectroscopy has been widely explored for non-invasive, early detection of NMSC as well as for evaluation of surgical margins before excision. Fluorescence-aided diagnosis is based on differences in spectral characteristics between healthy and neoplastic skin. Understanding the biological basis of such differences and correlating AF intensity to histological features could improve the diagnostic accuracy of skin fluorescence spectroscopy. The primary objective of the present pre-clinical ex vivo study is to investigate the correlation between the intensity of cutaneous AF and the histopathological features of NMSC. Ninety-eight lesions suggestive for NMSCs were radically excised from 75 patients (46 M; 29 F; mean age: 79 years). After removal, 115 specific reference points on lesions ("cases"; 59 on BBC, 53 on SCC and 3 on other lesions) and on peri-lesional healthy skin (controls; 115 healthy skin) were identified and marked through suture stitches. Such reference points were irradiated at 400-430 nm wavelength and resulting emission AF spectra were acquired through spectrophotometry. For each case, AFIR (autofluorescence intensity ratio) was measured as the ratio between the number of photons emitted at a wavelength ranging between 450 and 700 nm (peak: 500 nm) in

the healthy skin and that was captured in the pathological tissue. At the histological level, hyperkeratosis, neo-angiogenesis, cellular atypia, epithelial thickening, fibrosis and elastosis were quantified by light microscopy and were assessed through a previously validated grading system. Statistical correlation between histologic variables and AFIR was calculated through linear regression. Spectrometric evaluation was performed on 230 (115 cases + 115 controls) reference points. The mean AFIR for BCC group was 4.5, while the mean AFIR for SCC group was 4.4 and the fluorescence peaks at 500 nm were approximately 4 times lower (hypo-fluorescent) in BCCs and in SCCs than in healthy skin. Histological variables significantly associated with alteration of AFIR were fibrosis and elastosis ($p < 0.05$), neo-angiogenesis, hyperkeratosis and epithelial thickening. Cellular atypia was not significantly associated with alteration of AFIR. The intensity of fluorescence emission in neoplastic tissues was approximately 4 times lower than that in healthy tissues. Histopathological features such as hyperkeratosis, neo-angiogenesis, fibrosis and elastosis are statistically associated with the decrease in AFIR. We hypothesize that such tissue alterations are among the possible biophysical and biochemical bases of difference in emission AF between neoplastic and healthy tissue. The results of the present evaluation highlighted the possible usefulness of autofluorescence as diagnostic, non-invasive and real-time tool for NMSCs. (Figure. 6)

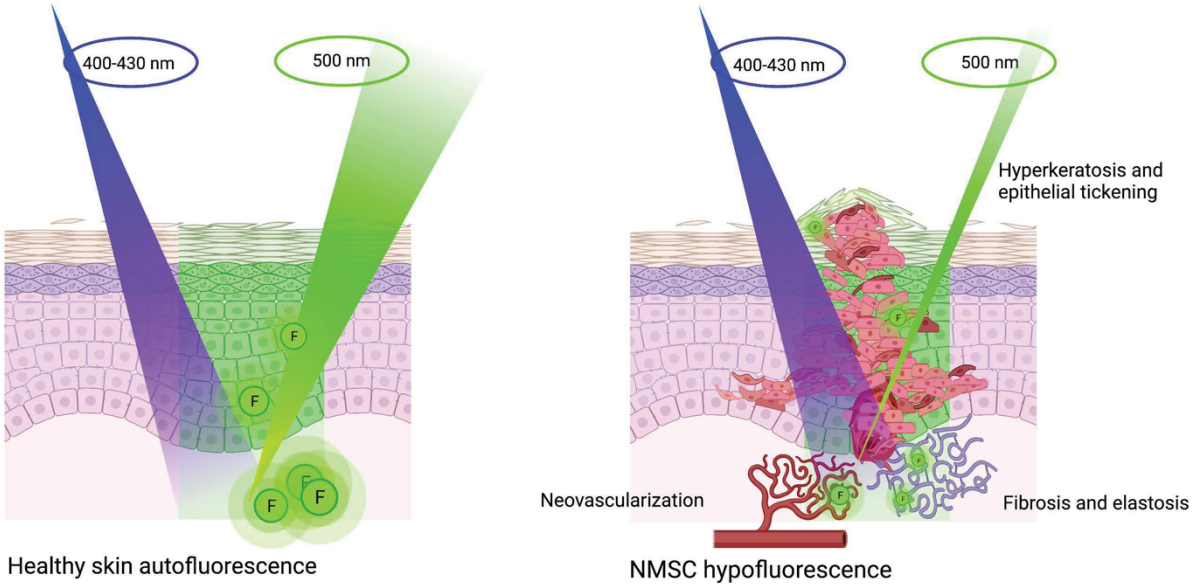

Figure 6: In this picture we can see a group of non melanoma skin cancer cells illuminated by a blue violet light of 400-430 nm, which absorb and re-emit light in the green spectrum. NMSC cells change the emission fluorescence spectra due to the variation of the major fluorophores of the skin.

3.2 Introduction

Non-melanoma skin cancer (NMSC) represents the most common cancer in fair-skin people. Basal cell carcinoma (BCC) accounts for approximately 75% of cases, the remaining mainly being squamous cell carcinomas (SCC)[25,26]. While BCC rarely metastasizes, metastases from high-risk SCCs are not uncommon and may be fatal [27,28,29,30,31].

Management of NMSC is based on early diagnosis and treatment, as well as monitoring of recurrences[32,23,22,33].

Several techniques, based on optical properties of skin, and including dermoscopy, reflectance confocal microscopy (RCM), multiphoton microscopy, fluorescence evaluation, diffuse reflectance and Raman spectroscopy, have been variously used as tools for non-invasive diagnosis of NMSCs[34,13,35]. Among these, dermoscopy and RCM are reliable techniques for melanoma diagnosis even if their efficacy for preoperative delineation of SCC surgical margins is questionable[36,37, 38,39].

Alteration of fluorescence (hyper and/or hypofluorescence) has been documented in neoplastic tissues, presumptively resulting from changes in the amount and distribution of fluorophores and in the chemico-physical properties of their environment[40]. In particular, modifications of collagen, elastin and NADH seem to account for the alteration of fluorescence observed in malignant tumors. Therefore, evaluation and measurement of AF could be a promising technique for non-invasive diagnosis and management of NMSCs[11,41].

Gross architectural alterations (e.g., hyperkeratosis, neoangiogenesis) associated with hyper- and hypofluorescence in pathologic tissues from the oral mucosa have been recently described[42]. Only a few other papers have been published in this field, and, to our knowledge, this is the first work on NMSC autofluorescence and its histopathological correlation[43].

The aims of the present study are 1. to investigate the differences in AF intensity between NMSC and healthy skin; 2. to analyze the histopathological determinants possibly accounting for AF alterations in pathologic skin.

3.3 Materials and Methods

Study Setting and Design

The study was conducted at the Policlinico of Modena, University of Modena and Reggio Emilia (Modena, Italy) from October 2019 to March 2020.

The study was a prospective, mono-centric, pre-clinical ex vivo study approved by the local Ethical Committee (n°1167.2018 Area Vasta Emilia Nord Ethical Committee, Policlinico di Modena, Via Largo del Pozzo 71, 41124). The research was conducted according to the Helsinki Declaration. All patients signed informed consent to the use of their data for research purposes.

AF Detection System

The AF detection system, (Figure 7) included:

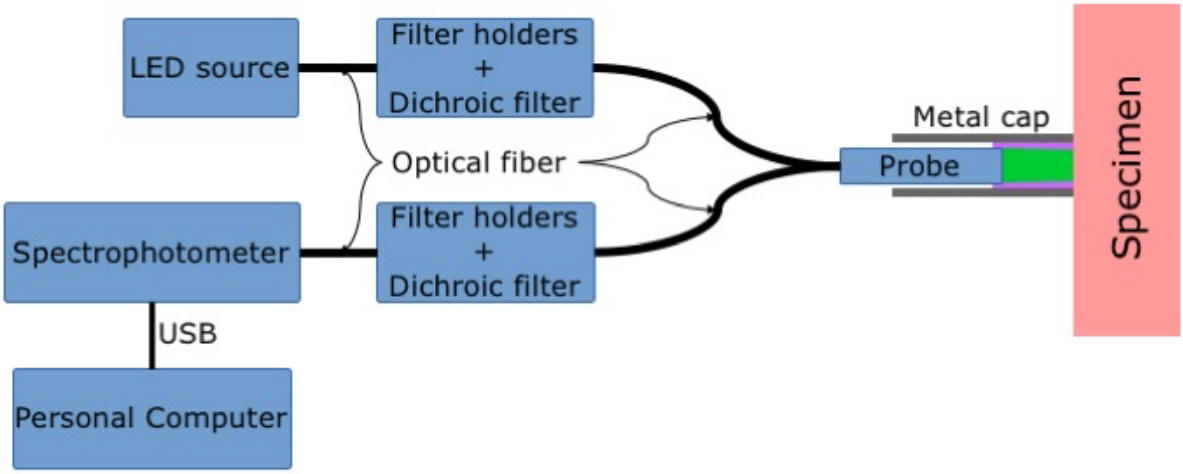

Figure 7 Basic representation of the AF detection system

(a) A LED source (LLS, Ocean Optics®, Dunedin, FL, USA), emitting light in the violet spectrum (400–430 nm), used to elicit AF in healthy and pathological skin;

(b) Dichroic filters (Thorlabs®, Newton, NJ, USA), used to select wavelengths either from the LED source and from captured skin AF;

(c)A bifurcated optical fiber (Ocean Optics®) to illuminate tissues and capture the AF;

(d) A spectrophotometer (Flame, Ocean Optics®), used to measure the spectrum of the captured AF emission light in the aforementioned range;

(e) A software application (SW) was also developed (in C language) and integrated into the AF detection system. The SW acquired and processed the captured AF spectra, which were then organized within a database (Figure. 7).

Study Population and AF Evaluation

Seventy-five (46 males (61%); 29 females (39%); mean age: 79 years (ranging from 42 to 93) consecutive subjects underwent preemptive routine skin surgery for lesions suggestive for NMSC. For every patient, clinical history was considered, in particular, smoking, diabetes, hypertension, autoimmune diseases and anticoagulant therapy.

Skin phototype was as follows: type II in 71 cases (95%) and type III in 4 cases (5%). Ten (13%) patients were smokers. Overall, 98 lesions were excised from the population study.

Forty-three (43.9%) lesions were located in the H-zone (high-risk zone: eyelids, eyebrow, periorbital region, nose, lip, chin, mandibular region, preauricular and retroauricular region, ear, temple, genitalia, hands and feet), 30 (30.6%) in the I-zone (intermediate-riskzone: cheeks, forehead, scalp, neck and pretibial region) (n = 30) and 25 (25.5%) in L-zone (low-risk zone: trunk and extremities).

One-hundred and fifteen lesional points were identified on the 98 excised specimens (ex vivo), and for each of these, a control point on clinically perilesional healthy skin was evaluated.

Lesional and control points were irradiated with a 400–430 nm excitation wavelength, and the emitted light was filtered in order to remove the reflected excitation light and to selectively isolate the AF emission. AF emission spectrum was measured by a spectrophotometer and then recorded.

The ratio between the number of photons emitted at 500 nm in the healthy skin and that emitted in the pathological tissue was utilized as a measure of AF (autofluorescence intensity ratio AFIR).

AFIR > 1 indicates a decrease in AF, while AFIR < 1 indicates an increase in AF.

After evaluation, all points were marked through suture stitches as reference for histologic analysis (Figure. 8).

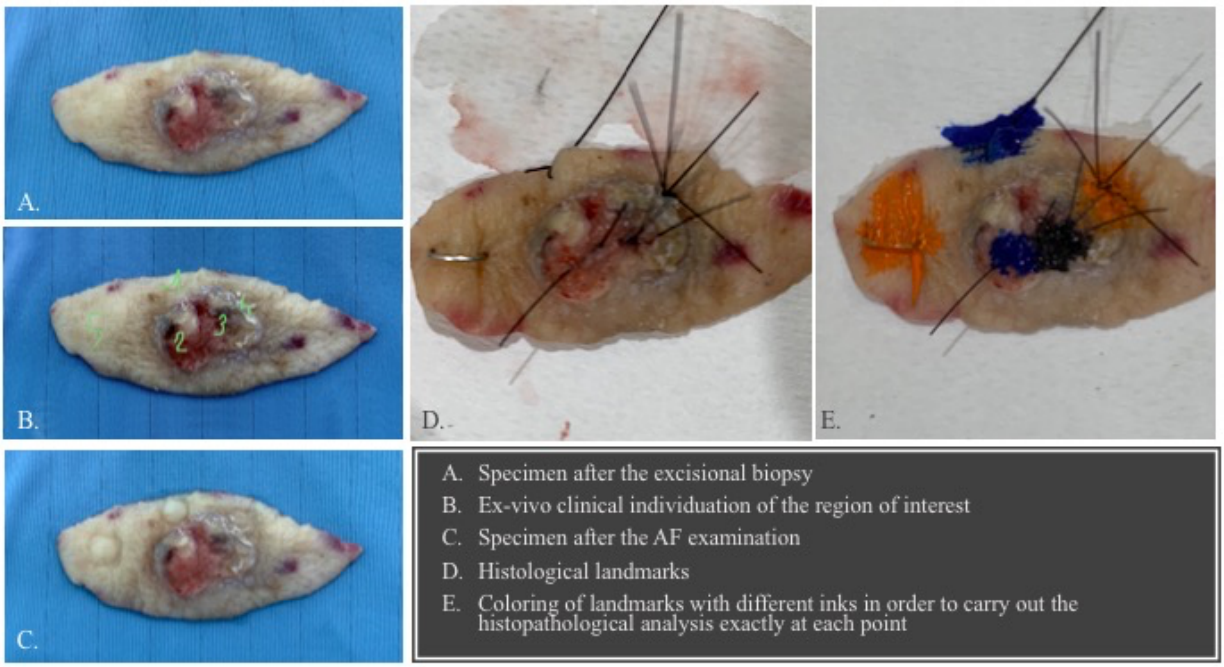

Figure 8. Example of lesional and healthy skin reference points on excised specimen: (a) specimen after excisional biopsy; (b) ex vivo identification of control points (1,5) and lesional points (2,3,4) for 400–430 nm irradiation; (c) suture stitches as reference for histologic analysis, (d) tissue marking dyes before histopathological examination.

Histologic analysis of the marked points was performed on the basis of histopathological diagnosis. BCCs were subclassified into: superficial, nodular, morpheiform and pigmented. Lesions in the SCC group were subclassified into in situ SCC, Bowen disease, infiltrative SCC and keratoacanthoma. Actinic keratoses were included in the SCC group.

Histological Variables

The histopathological determinants evaluated for each diagnosis of NMSC and their degrees were the following:

1. Hyperkeratosis (absent (0), mild (1), moderate (2) and severe (3));
2. epithelial thickening (defined as an increased distance between the corneum and the basal layer) (absent (0), mild (1), moderate (2), severe (3) and with presence of ulcer (4));
3. Fibrosis (absent (0) and present (1));
4. Elastosis (absent (0) and present (1));
5. Neovascularization (absent (0), mild (1), moderate (2) and severe (3));
6. Cellular atypia (absent (0), present with grade 1, 2 or 3).

Each histopathological variable was correlated to AFIR.

Statistical Analysis

Data analysis was performed using the commercial package IBM SPSS Statistics for Windows (version 22, IBM Corp., Armonk, NY) and the open-source statistical system Jamovi v.1.8.4 (The jamovi project (2021). jamovi. (Version 1.8) [Computer Software]. Retrieved from https://www.jamovi.org, accessed on 30 June 2021, based on the R system. Measures of central tendency, dispersion and shape were calculated for all the variables in the data set. Summaries included arithmetic mean, median, standard deviation, interquartile range, minimum, maximum, asymmetry, kurtosis and the relevant standard errors and 95% confidence intervals. Normality of the data was

tested by the Shapiro–Wilk test. Categorical data were reported in frequency tables and expressed as absolute, relative and cumulated frequencies and percentages.
Univariate comparisons between continuous variables were performed using both parametric tests (Student's t-test, ANOVA) and non-parametric test (Mann–Whitney's U-test, Kruskal–Wallis test). Comparisons between categorical variables in contingency tables were performed using the chi-square test and Fisher's exact test.
The combined effects of different predictors on outcome variables were tested by multiple linear regression. The results were considered statistically significant for a p-value less than 5% ($p < 0.05$).

3.4 Results

AF Measurement in NMSC and Healthy Skin

The number of excised lesions suggestive of NMSC was 98.
All the control points on healthy skin showed an emission spectrum ranging between 450 and 700 nm (peak at 500 nm). Evaluation of all the 115 lesional points highlighted an alteration in AF (mean: 4.433; median: 3.3277). Histological analysis confirmed that almost all the areas characterized by the loss of AF were NMSC, subclassified as follows: 59 (51.3%) BCC, 53 (46.1%) SCC, and 3 (2.6%) benign lesions. Each point clinically indicated as control received a histological description of "healthy skin" (Figure. 9).
All the BCC cases (100%) and 47 (90.4%) SCC cases out of 53 showed a decrease in AF. In particular, the mean AFIR of BCC was 4.5, indicating that, at 500 nm, BCCs are in average 4.5 times less fluorescent than healthy skin. Similarly, mean AFIR of SCC was 4.4 (Figure10)
No statistically significant differences between the mean of AFIR in BCC and SCC groups were detected (Student's t $p = 0.170$; Mann–Whitney U $p = 0.143$).

AFIR of BCC and SCC histological subtypes as well as the lowest and highest values recorded are summarized in Table 1 and Table 2.

Table 1: Mean AFIR among different BCC subtypes

BCC subtype	Mean AFIR ratio	Minimum	Maximum	Standard deviation	Standard error
Superficial	2.6	1.435	5.749	1.358	0.4802
Nodular	4.4	1.354	16.10	3.437	0.5014
Morpheiform	4.8	3.607	6.082	1.750	1.237
Pigmented	12.8	9.908	15.73	4.120	2.913

Table 2: Mean AFIR among different SCC subtypes

SCC subtype	Mean AFIR ratio	Minimum	Maximum	Standard deviation	Standard error
Keratoacanthoma	1.8	1.296	2.240	0.6674	0.4719
In situ SCCs	2.3	1.250	3.286	0.7685	0.2717
Bowen disease	5.0	1.342	12.98	4.173	1.391
Infiltrative SCCs	5.1	0.5689	15.63	3.482	0.6723
Actinic keratoses	4.1	0.4823	18.02	5.805	2.052

Figure 9. (A): Example of clinicopathological correlation of AF alteration in BCC: (a) identification of control point (1) and lesional point (2) on the excised specimen (b) histopathological section (hematoxylin and eosin, 4x magnification) corresponding to point 1 healthy skin, and histopathological section (hematoxylin and eosin, 4_xmagnification) corresponding to point 2 (infiltrating BCC) (c) AF emission spectra of point 1 and point 2. (d) absolute spectra of the two points (B): Example of clinicopathological correlation of AF alteration in SCC: (a) identification of control (1) and lesional points (2); (b) histopathological section (hematoxylin and eosin, 4x magnification) corresponding to point 1 (healthy skin), and histopathological section (hematoxylin and eosin, 4_xmagnification) corresponding to point 2 (poorly differentiated SCC) (c) AF emission spectra of point 1 and point 2, (d) absolute spectra of the two points.

(A)

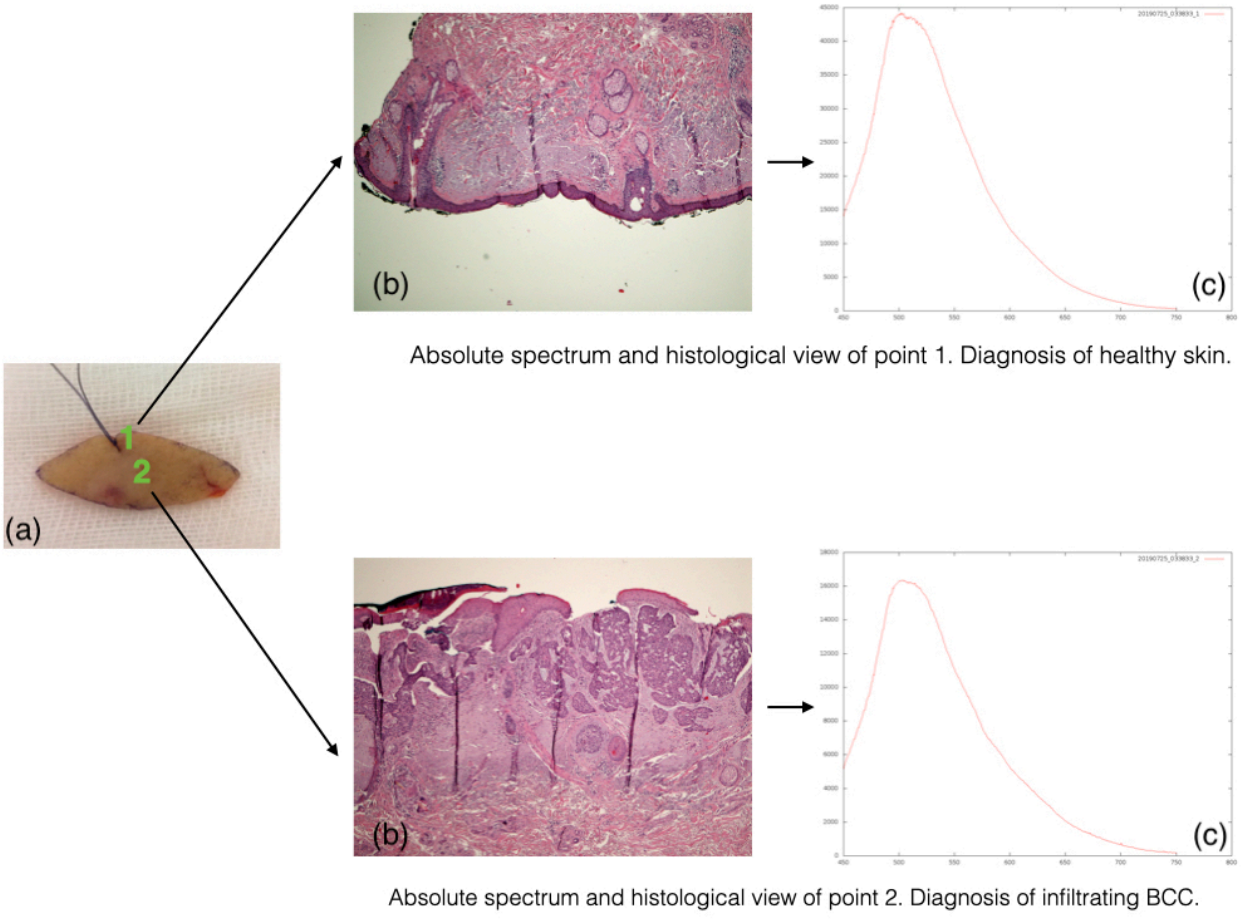

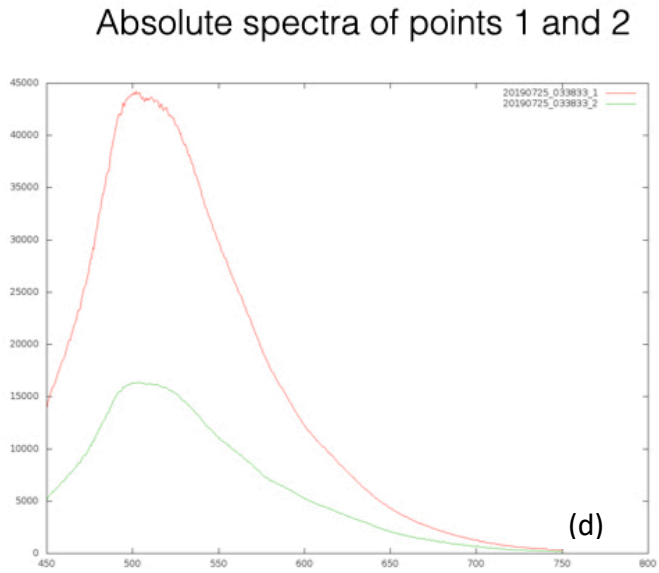

(B)

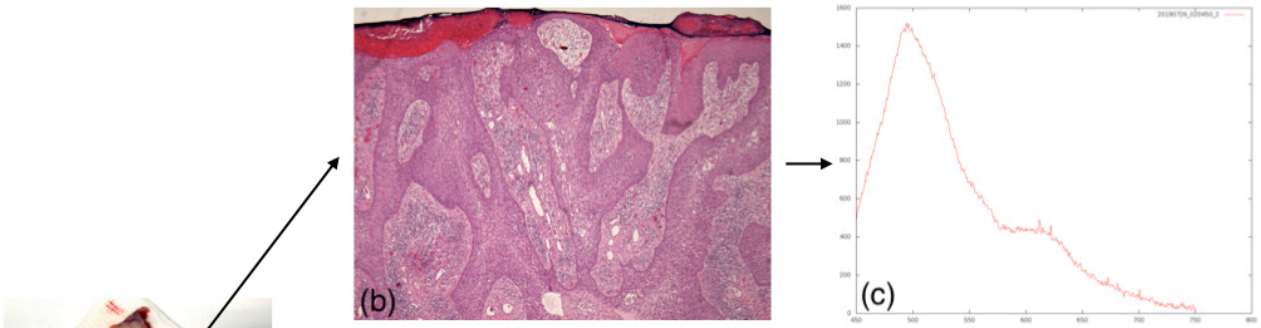

Absolute spectrum and histological view of point 2. Diagnosis of poorly differentiated SCC.

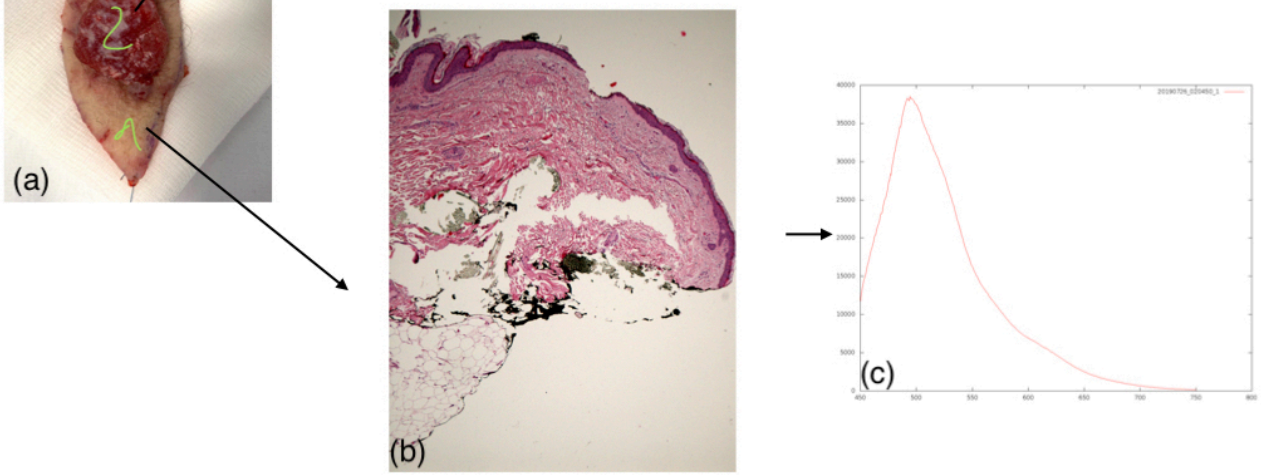

Absolute spectrum and histological view of point 1. Diagnosis of healthy skin.

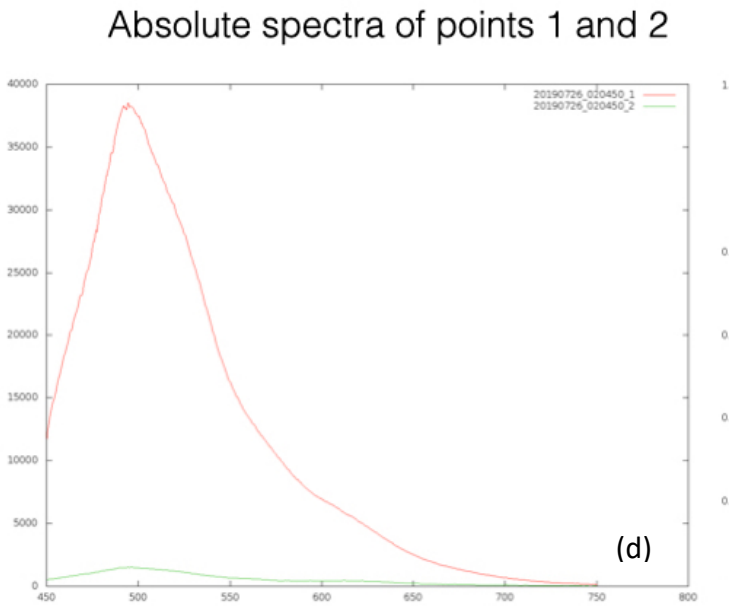

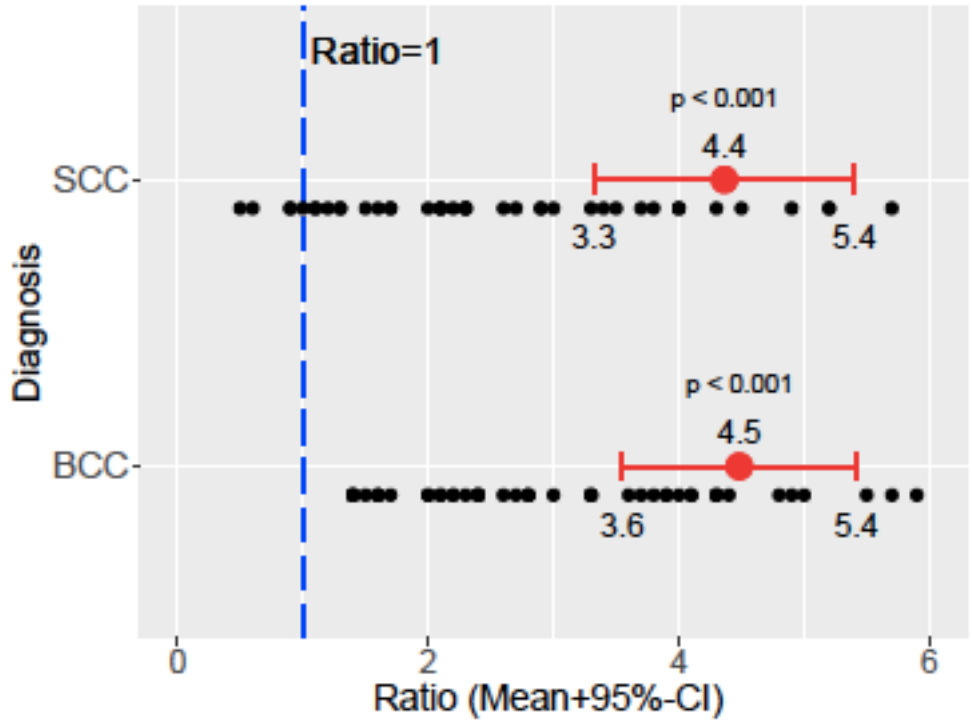

Figure 10. Autofluorescence intensity ratio in a group of NMSC (BCC and SCC)

Histopathological Results

Fibrosis and Elastosis

Fibrosis was statistically associated with alteration of AFIR. The mean AFIR varied from 3.3 to 4.7 in cases of fibrosis presence (p = 0.047) (Table 3 and Table 4).

Table 3 Descriptive statistics for the variable "Fibrosis". AFIR autofluorescence intensity ratio; SD standard deviation; SE standard error.

Group Descriptives (Fibrosis)

	Group	N	Mean	Median	SD	SE
Intensity ratio	absent	16	3.309	2.164	3.130	0.7825
	present	99	4.676	3.521	3.734	0.3753

Table 4 Indipendent samples comparisons (Absent, Present) for the variable "Fibrosis".

Independent Samples T-Test (Fibrosis)

		Statistic	df	p
Intensity ratio	Student's t	-1.386	113.0	0.168
	Mann-Whitney U	546.0		**0.047**

A similar variation in AFIR was observed in the presence of elastosis, even if no statistical association could be highlighted (see Table 5 and Table 6).

Table 5 Descriptive statistics for the variable "Elastosis".

Group Descriptives (Elastosis)

	Group	N	Mean	Median	SD	SE
Intensity ratio	absent	89	4.230	3.295	3.322	0.3521
	present	26	5.361	3.054	4.659	0.9138

Table 6 Indipendent samples comparisons (Absent, Present) for the variable "Elastosis"

Independent Samples T-Test (Elastosis)

		Statistic	df	p
Intensity ratio	Student's t	-1.386 [a]	113.0	0.169
	Mann-Whitney U	1070		0.563

[a] Levene's test is significant (p < .05), suggesting a violation of the assumption of equal variances

In cases where fibrosis and elastosis coexisted, AFIR increased, reaching a value of 7.7.

Hyperkeratosis

In the case of absence of hyperkeratosis, mean AFIR was 4.8; when hyperkeratosis was scored as 1, 2 and 3, mean AF intensities were 4.4, 4.5 and 1.5, respectively. The Kruskal-Wallis test showed a statistically significant difference among the groups (p = 0.034) (Table 7). Pairwise comparisons revealed that the significance was imputable to the absence and grade 3 hyperkeratosis (p = 0.016) (Table 8).

Table 7 Kruskal-Wallis test and pairwise comparisons for the variable "hyperkeratosis"

One-Way ANOVA (Non-parametric) - **Hyperkeratosis**			
Kruskal-Wallis			
	χ^2	df	p
Intensity ratio	8.686	3	**0.034**

Table 8 Dwass-Steel-Critchlow-Fligner pairwise comparisons (intensity ratio) for the variable "hyperkeratosis" after statistically significant Kruskal- Wallis test. Column 1 and Column 2 represent the paired hyperkeratosis scores comparison.

Dwass-Steel-Critchlow-Fligner pairwise comparisons – intensity ratio			
		W	p
0	1	-0.27054	0.998
0	2	-0.01111	1.000
0	3	-4.18994	**0.016**
1	2	0.04837	1.000
1	3	-3.22125	0.103
2	3	-3.63054	0.050

Epithelial Thickening

No epithelial thickening was detected in 56 samples; while 9 samples displayed grade I, 28 grade II, 2 grade III and 20 grade IV thickening.

The Kruskal-Wallis test showed a statistically significant difference among the groups, when comparing presence or absence of epithelial thickening mean AFIR 4.2 Vs 4.78, p = 0.038) (Table 9).

In particular, in cases without epithelial thickening, the AFIR was 4.2; in grade 1 thickening, 3.9; in grade 2, 4; in grade 3, 2.4; and in grade 4, 6.5. In particular, pairwise comparisons revealed that significant differences might be between absence and grade 4 epithelial thickening (p = 0.056) (Table 10).

Table 9 Kruskal-Wallis test for the variable "epithelial thickening"

One-Way ANOVA (Non-parametric) – **Epithelial thickening**			
Kruskal-Wallis			
	χ^2	**df**	**p**
Intensity ratio	10.16	4	**0.038**

Table 10 Dwass-Steel-Critchlow-Fligner pairwise comparisons (intensity ratio) for the variable "epithelial thickening" after statistically significant Kruskal- Wallis test. Column 1 and Column 2 represent the paired epithelial thickening grades in comparison

Dwass-Steel-Critchlow-Fligner pairwise comparisons – intensity ratio			
		W	**p**
0	1	-0.99385	0.956
0	2	-0.04026	1.000
0	3	-0.96425	0.961
0	4	3.79521	**0.056**
1	2	0.70088	0.988
1	3	-1.00000	0.955
1	4	3.20000	0.157
2	3	-0.70548	0.988
2	4	3.63763	0.076
3	4	2.42272	0.426

Neovascularization

In cases without neovascularization the mean AFIR was 2.1; in grade 1, 4.6; in grade 2, 6.4; and in grade 3, 4.8. The Kruskal-Wallis test showed a statistically significant difference among the groups (p = 0.019) (Table 11). In particular, pairwise comparisons revealed statistically significant differences between absent neovascularization and grade 1 neovascularization (p = 0.016) (Table 12).

Table 11 Kruskal-Wallis test and pairwise comparisons for the variable "neovascularization"

One-Way ANOVA (Non-parametric) – **Neovascularization**			
Kruskal-Wallis			
	χ^2	df	p
Intensity ratio	9.989	3	**0.019**

Table 12 Dwass-Steel-Critchlow-Fligner pairwise comparisons (intensity ratio) for the variable "neovascularization" after statistically significant Kruskal- Wallis test. Column 1 and Column 2 represent the paired neovascularization grades in comparison

Dwass-Steel-Critchlow-Fligner pairwise comparisons – intensity ratio			
		W	p
0	1	4.1995	**0.016**
0	2	3.2451	**0.099**
0	3	2.7520	0.209
1	2	1.6459	0.650
1	3	-0.7508	0.952
2	3	-1.3799	0.763

Cellular Atypia

In cases without cellular atypia, AFIR was 4.5; in grade 1 atypia, 3.8; in grade 2, 5.8; and in grade 3, 4.4. Kruskal-Wallis test was not statistically significant (p = 0.334) (Table 13).

Table 13 Kruskal-Wallis test and pairwise comparisons for the variable "cellular atypia"

One-Way ANOVA (Non-parametric) – **Cellular atypia**			
Kruskal-Wallis			
	χ^2	df	p
Intensity ratio	3.396	3	0.334

Multivariate Analysis

Multivariate analysis by a multiple linear regression model was used to analyse all histological determinants together in order to evaluate which were significant in influencing AFIR (Table 14).

Table 14 Results of multiple linear regression including all histological variables as predictors. Dependent variable: AF intensity ratio.

Model Coefficients – intensity ratio

Predictor	Estimate	SE	t	p
Intercept [a]	-1.36559	1.633	-0.83614	0.405
1) **Fibrosis**:				
present – absent	2.95274	1.331	2.21771	**0.029**
2) **Elastosis**:				
present – absent	2.67802	1.071	2.50069	**0.014**
3) **Neovascularization**:				
1 – 0	2.69778	1.098	2.45708	**0.016**
2 – 0	4.17302	1.539	2.71197	**0.008**
3 – 0	3.00542	1.339	2.24429	**0.027**
4) **Epithelial thickening**:				
1 – 0	-0.28104	1.332	-0.21107	0.833
2 – 0	-0.50670	1.298	-0.39037	0.697
3 – 0	-1.04651	2.774	-0.37731	0.707
4 – 0	0.97872	1.033	0.94719	0.346
5) **Hyperkeratosis**:				
1 – 0	-0.04351	1.260	-0.03454	0.973
2 – 0	-0.63988	1.015	-0.63038	0.530
3 – 0	-3.42011	1.714	-1.99522	**0.049**
6) **Cellular atypia**:				
1 – 0	1.06353	1.178	0.90300	0.369
2 – 0	1.46131	1.174	1.24451	0.216
3 – 0	0.71902	1.455	0.49424	0.622

[a] Represents reference level

When considered together, significant variables for AFIR were (presence/absence of) fibrosis, elastosis, neovascularization (absent versus grade 1, 2 and 3) and hyperkeratosis (absent versus grade 3). Epithelial thickening and cellular atypia were not statistically significant according to the linear regression model.

Clinical variables were also included in the regression, but none of these (smoking, diabetes, hypertension, autoimmune disease or anticoagulant therapy) were significantly correlated with the degree of fluorescence of the lesion. A statistically significant correlation emerged between hypertension and elastosis ($p = 0.021$), since 85% of patients had both hypertension and elastosis.

3.4 Discussion

Despite the development of several adjunctive diagnostic aids which can possibly help the clinician in the pre-operative differentiation between benign and malignant lesions, the definitive diagnosis of the vast majority of skin conditions requires histopathological analysis. In case of doubts, the collection of one or more specimens through biopsies is the gold-standard procedure that allows the planning of an appropriate treatment[44].

As some malignant tumors (e.g., NMSCs in the early phases of development) can mimic benign lesions, the availability of a reliable, non-invasive, highly specific and sensible tool able to identify peculiar features suggestive of malignancy would provide strong input to the management of skin diseases.

Within this context, and following previous analyses performed on other anatomical sites (e.g., oral cavity)[42,45,46], we designed and conducted the present study, which attempts to evaluate the usefulness of AF for the diagnosis and the management of a heterogeneous group of NMSCs.

To date, different excitation wavelengths have been applied to fluorescence spectroscopy of the skin and in particular high-energy wavelengths in the UV region. It is known that wavelengths in the UV region, in addition to AF generation, induce oxidative stress in cells, resulting in modifications in the cellular redox state, damage to the cell structures and cell death[47]. Based on recent observation, for the present study, we selected a 400–430 excitation wavelength in the blue region of visible light[48].

The results of the present analysis demonstrate that all ex vivo specimens harbouring neoplastic alterations at the histological level show a marked alteration of AF compared to perilesional, histologically healthy skin.

Such alterations can take the form of AF enhancement or AF reduction and are invariably present, conferring a specific optical appearance of NMSCs. In the present

analysis, the vast majority of cases displayed a marked decrease in AF, which was on average 4.4–4.5 times lower than that of clinically healthy skin.

The decrease in AF in NMSCs after 400–430 excitation is in line with data already present in the literature[13,49,50,51]. In 2002, Panjehour et al. highlighted that healthy skin exhibited a stronger fluorescence emission than BCC and SCC when excited at 410 nm[52].

Assessment of AFIR in different BCCs and SCCs histological subtypes showed a trend to decline not statistically significantly but directly proportional to tumor thickness and infiltration. This suggests a different fluorophore distribution between healthy and lesional skin, in line with previous findings[11,50,53].

The histological analysis showed a correlation between histological variables and AF alteration. Our data show that fibrosis and elastosis (present vs. absent), neoangiogenesis (absent vs. present with grades 1, 2 and 3), hyperkeratosis (absent versus present with grade 3) and epithelial thickening (absent vs. present with grades 1, 2, 3 and 4) were significantly associated with alteration of AF. Cellular atypia was not significantly associated with alteration of AF.

As previously demonstrated by clinical and histological studies conducted on the oral mucosa the main fluorophores within the range of 400–460 nm are NADH and FAD cellular coenzymes, collagen and elastin[54]. These data may support the hypothesis that the positive association between the presence of fibrosis and elastosis with the decrease in AF can be due to alteration in the distribution and concentration of these fluorophores[53,54].

The presence of epithelial thickening, conditions characterized by an increased distance between the corneum and the basal layer, is associated with a higher decrease in AF when compared to the normal epidermis. A thickened epithelium can probably obstruct the penetration of specific wavelengths in deep dermal layers, where the main known fluorophores are located.

Last, the presence of neovascularization was also associated with a decrease in AF. In this case, the decrease of AF can be influenced by hemoglobin reabsorption of the fluorescence from deeper dermal layer[55,56].

Previous studies demonstrated the correlation between AF intensity and skin phototype. Fluorescence-based methods have higher specificity and sensibility when applied to fair-skinned people[52]. Our study population is rather homogeneous with a phototype II in almost all cases evaluated (95%), thus allowing an unbiased interpretation of the results.

As extensively described in the literature, other "optical biopsy" techniques such as dermoscopy and confocal microscopy have been demonstrated to improve diagnostic accuracy in NMSC[38].However, dermoscopy and/or confocal imaging are used for the assessment of surgical margins either for BCC and lentigo maligna, while no evidence still exists about potential benefits of these techniques for SCCs[36, 37].

4 Comparative study of in-vitro autofluorescence of normal versus non-melanoma-skin-cancer cells at different excitation wavelengths

4.1 Background

In this experimental study the autofluorescence of squamous carcinoma cells, stimulated by 6 different excitation wavelengths in the range 280–533 nm, has been compared with the autofluorescence of normal control keratinocytes. Skin cells were cultivated in vitro, to isolate their characteristic autofluorescence form the more complex one that would be originated by the complete skin tissue. Autofluorescence spectra in the visible range were complemented by absorption measurements. It was observed that the control cells showed characteristic emission (and absorption) structures due to typical endogenous chromophores [FAD and NAD(P)H, lipo-pigments, porphyrins], that were severely dumped in pathological cells. The autofluorescence spectra were then elaborated by multivariate analysis: after a first exploratory data analysis by means of Principal Component Analysis, the whole dataset was used to develop classification models using partial least squares-discriminant analysis, to differentiate between normal and pathological cells. This permitted us to identify the most suitable fluorescence spectral interval, in the 550–670 nm range, to discriminate between normal and pathological behavior, independently of the excitation wavelength.

4.2 Introduction

Optical luminescence for diagnostic purposes in medicine is a well-developed field [9, 40]. Techniques based on the detection of luminescence are fast, noninvasive, and quantitative. Fluorescence at certain wavelengths can be typically induced in tissues by treating them with fluorescent markers that bind to selected receptors. Besides this, the study of intrinsic fluorescence [autofluorescence (AF)] of different bio-molecules is becoming more and more important. AF of specific cells, matrices and bio-molecules is strictly related to their morpho-functional properties. Alterations of these properties, for example, due to pathologies like tumors, can induce strong modification of AF[57,49,42,52,58,11]. Most important endogenous fluorophores are molecules largely present in living systems, like structural proteins, aromatic amino acids, enzymes, flavins, lipopigments, porphyrins, collagen and elastin fibers, to cite some[9,57,47,59]. After excitation with monochromatic light at specific wavelength, these systems emit characteristic luminescence at higher wavelengths. The spectral line shape and intensity of the different spectral regions depend on the bio-molecules and their concentration. On the other hand, in most cases the recorded signals are complicated: not only because the line shapes of the specific fluorophores are broad and are partially superimposed, but also because multiple fluorophores are typically present, adding up their contributions.

Due to its clear potential, the field is in rapid expansion. Most studies are carried out directly in vivo, where the signal is complicated further, due to the contribution of different emitters: fluorophores inside cells, in the connective tissue and from the blood/fluids. Moreover, a great variability can be found in different individuals or in different sampled regions of the same individual. Moreover, a pathological alteration can affect the contributions from the constituents in a different way, making the analysis intricate.

In the present study we focus our attention on AF produced by isolated skin cells grown in vitro, comparing the signal of non-cancerous versus neoplastic keratinocytes [squamous cell carcinoma (SCC)].. A critical factor for dermatologists is the early diagnosis, to provide proper treatment. Surgical excision with clear margins represents the best approach to reduce the rate of recurrence. AF spectroscopy would provide a powerful and fast diagnostic tool to guide the correct early treatment of the affected areas of the skin [50]. It was recently demonstrated that AF spectroscopy can be used as an optical biopsy tool, for the early detection of NMSC ex vivo [60]. It was found that the overall intensity of the fluorescence emission in NMSC tissues reduced sizably compared to tissues in healthy conditions. The present study extends this investigation, focusing on the sole contribution of keratinocytes. This type of study, where single contributors to luminescence are considered, is still quite rare in the literature.

AF was measured both on cell pellets and normal saline cell suspension (PBS) at different wavelengths of the excitation light. In particular, commercially available light emitting diodes (LEDs) were adopted as excitation sources, working at λ_{exc} = 280, 310, 365, 405, 470, and 533 nm.

Multivariate analysis of the emitted fluorescence spectra was then performed to get quantitative information, to provide a method that clearly disentangles normal and pathological situations and to emphasize those spectral regions that appear more meaningful as far as the classification between normal and cancerous cells is concerned. Multivariate analysis-based approaches for the differentiation between AF spectra measured on healthy and cancer cells have already been successfully applied in the literature [61,12,57]. In the present study, multivariate analysis of the AF spectra was performed in two subsequent steps. The first step consisted in an unsupervised exploratory analysis performed by calculating principal component

analysis (PCA) models separately for each group of AF spectra measured at a given excitation wavelength. Then, in the second step, all the AF spectra measured at the six excitation wavelengths were merged in a unique dataset and subjected to multivariate classification by means of partial least squares-discriminant analysis (PLS-DA). Different spectra preprocessing methods were tested, and the corresponding classification models were validated by means of an external test set. The performance of the best performing classification model was also further verified by means of a permutation test.

Hypofluorescent aspect of cutaneous neoplasms[60], has been already demonstrated, however, several well-known dermal and epidermal chromophores could give reason of such findings (e.g., hemoglobin, collagen, keratins of the stratum corneum); therefore, whether cancerous cells specifically could be (or, at least, partially) responsible for NMSC hypofluorescence remained to be clarified [42,54]. The goal of the present study is to assess AF changes in SCC cells compared to healthy keratinocytes, in the absence of possible adjacent tissue interferences.

4.3 Experimental section

Cell cultures

UPCI:SCC154 cell line was used for in vitro evaluation of the behavior of tumoral cells from tongue squamous cell carcinoma (SCC). Cells were HPV+, P53neg.

Control keratinocytes (primary cells) were obtained from cutaneous discarded material from different donors undergoing elective surgery at Dermatologic Surgery Unit, Modena University Hospital. In particular, 3-donor pool keratinocytes were initially co-seeded with mitomycin-treated 3 T3 murine fibroblasts to promote epithelial cell growth.

Cells were plated into 75 cm^2 culture flasks at a density of 10^6 cells/flask. Trypan blue was used for the assessment of cell viability. To increase the luminescence signal form cells and avoid signal contamination due to the culture solution, AF was measured on cell pellets. The pellets were then put on a suitable support (see below) and care was taken in acquiring AF immediately after removing the cells from the solution, in order to minimize deterioration.

Optical setup

Fluorescence spectra were recorded with an Ocean Insight QEPRO-FL high sensitivity spectrometer working in the wavelength range between 348 and 1132 nm. High power LEDs from Ocean Insight (model LSM LEDs) were used as excitation sources, with emission wavelengths centered at 280, 310, 365, 405, 470, and 533 nm, FWHM <20 nm (36 nm for λ_{exc} = 533 nm). Solarization-resistant UV–visible optical fibers were used to transport light to the cell samples and to collect the luminescence signal and send it to the spectrometer. A sketch of the experimental apparatus is shown in Figure 11ab. In Figure 11a the configuration used to measure luminescence from the cell pellets is reported. A solarization-resistant coaxial reflection/backscattered probe was used. Cell pellets were deposited on a Petri plastic transparent dish with a black light-absorbing paper placed on the back, to reduce luminescence contributions from scattered light on the dish support. The support was custom designed to allow for a variable tilt angle between the impinging/collection direction and the Petri plate, to avoid a direct reflection of the incident excitation light in the collection channel and reduce possible AF phenomena from the optical fiber itself. A system to control precisely the probe height with respect to the sample was also implemented, to reproduce strictly the sampling geometries for the different replicas of the cell samples. Care was taken to disentangle the luminescence signal of the cells from the

possible contribution of the support. Different supports were therefore tested (plastic Petri dishes, Eppendorf test tubes, multi-wells), at different incidence and detection angles. Petri transparent dishes, with the black light-absorbing paper positioned at the back and at a tilt angle of 30° were seen to provide the best results in terms of negligible incident light backscattering and negligible luminescence from the sample holding system. An interferential, high pass, linear variable filter (Ocean Insight, model LVF-H) was also used to cut the excitation wavelength in the measurement channel and to avoid saturation of the spectrometer.

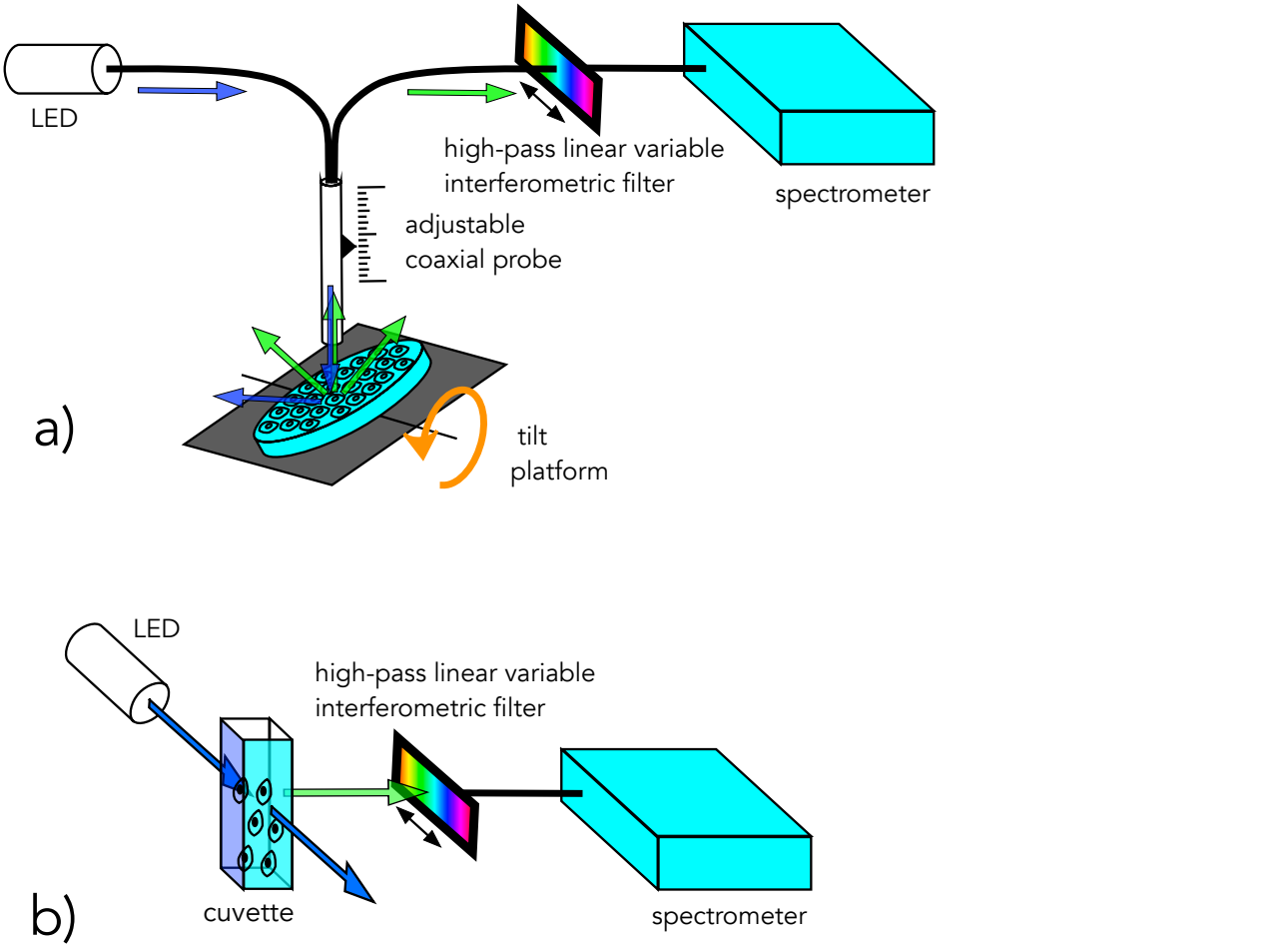

FIGURE 11. (a) Scheme of the experimental apparatus used to measure fluorescence from cells deposited on a Petri dish. (b) Scheme of the apparatus used to measure fluorescence from cells in liquid suspension.

Figure 11b illustrates the configuration adopted to measure the luminescence of suspended cells in normal saline solution (0.9%). In this case, quartz optical cuvettes were used, and light was collected at perpendicular direction with respect to the impinging beam.

Transmission spectra were also recorded to flank the luminescence results, using a balanced deuterium and tungsten halogen source (DH-2000-BAL Light Source from Ocean Insight) and a miniature spectrometer (USB4000-XR1 from Ocean Insight). Cells supported on a transparent Petri dish were used for transmission experiments.

Multivariate analysis

The set of AF spectra measured over a period of 7 months on cells deposited on Petri dishes, which were considered due to the higher signal-to-noise ratio with respect to the spectra measured in solution, was subjected to multivariate analysis.

Each spectrum contains the intensity values measured at 1044 wavelengths in the range between 348 and 1132 nm. The dataset includes all the spectra acquired using the six different excitation wavelengths; in particular, eight spectra (four on healthy samples and four on NMSC samples) measured for each one of the 280, 310, and 365 nm excitation wavelengths, and seven spectra (four on healthy samples and three on NMSC samples) measured for each one of the 405, 470, and 533 nm excitation wavelengths.

Separate PCA models for each excitation wavelength

As a first step, each group of spectra measured at a given excitation wavelength was explored separately from the others by means of PCA, which is an unsupervised technique used to reduce the data dimensionality while preserving the original structure of the dataset. In the present work, PCA was used to evaluate whether, for each excitation wavelength, the pattern of the corresponding emission spectra of healthy samples was somehow different from the pattern of the spectra measured on NMSC samples, thus without forcing any separation between the two classes.

To this aim, for each group of spectra measured at a given excitation wavelength, two PCA models were calculated, corresponding to two variable preprocessing methods: mean centering and autoscaling. Mean centering consists in transforming each variable by subtracting its mean value from all the observations, while autoscaling consists in mean centering and then dividing by the variable standard deviation.

In addition to assessing whether differences were observable between healthy and NMSC samples, PCA also allowed to investigate which excitation wavelengths led to the best separation between the two classes, and to identify the most relevant spectral regions.

PLS-DA classification models on the whole dataset

The second step of multivariate analysis consisted in calculating classification models on the whole dataset of spectra, in order to evaluate the possible presence of

common spectral regions for all the excitation wavelengths where the AF spectra present different patterns for healthy and NMSC cells. The whole dataset, including 24 spectra measured on healthy cells and 21 spectra measured on NMSC (SSC) cells, was analyzed by means of PLS-DA. To this aim, the dataset was first randomly divided in a training set including 30 spectra and in a test, set including the remaining 15 spectra, taking care to include spectra for each excitation wavelength and each class in both the training and the test set, as reported in Table 15.

The training set was then used to calculate two PLS-DA models, one considering mean centering and one considering autoscaling as preprocessing method. The optimal dimensionality of each PLS-DA model, that is, the number of Latent Variables (LVs) leading to the minimum classification error, was selected by random cross validation, which was performed subdividing the training set samples in five deletion groups and repeating the cross validation for 20 iterations. Both the models were then validated by means of the test set samples. The classification performance of the PLS-DA models was evaluated considering their classification efficiency (EFF), calculated as the geometric mean of sensitivity (SENS) and specificity (SPEC). SENS is the percentage of samples of the modelled class correctly accepted by the class model, SPEC is the percentage of objects of the other classes correctly rejected by the class model, and EFF is the geometric mean of SENS and SPEC. Since for a two-class PLS-DA model like in the present case (healthy and NMSC classes) the SENS value of class 1 is equal to the SPEC value of class 2, and the SPEC value of class 1 is equal to the SENS value of class 2, the EFF value for both the classes is the same. The EFF, SENS, and SPEC parameters were computed considering the values calculated on the training set (EFFCAL, SENSCAL, SPECCAL), those estimated in cross validation (EFFCV, SENSCV, SPECCV), and the values predicted for the test set (EFFPRED, SENSPRED, SPECPRED).

Considering the relatively limited number of AF spectra available to perform multivariate classification, to further verify the statistical significance of the PLS-DA model showing the best overall performance, a permutation test was also implemented. The permutation test essentially consisted in repeatedly and randomly reassigning the samples to the two classes, both for the training and for the test set. For each one of the 100 permutations considered in the present work, a PLS-DA model was calculated on the training set considering the same number of LVs of the correct model and the same cross validation procedure, and then it was applied to the test set. For each permutation, the values of EFFCAL, EFFCV, and EFFPRED were calculated. Finally, the distributions of the EFFCAL, EFFCV, and EFFPRED values of the 100 permutations were compared with the corresponding values of the correct model, using a one-tailed t test to verify whether its EFF values were statistically significant ($p = 0.05$).

The PCA and PLS-DA models were calculated using the functions available in the PLS-Toolbox ver. 8.9.2 (Eigenvector Research Inc., Manson, WA, USA) running in the Matlab ver. 9.10 (R2021a) environment (The MathWorks Inc., Natick, MA, USA). The permutation test was calculated using a Matlab function written ad hoc.

4.5 Results and Discussion

AF spectra

AF spectra were recorded for different batches of the normal and SSC cells. In spite that extreme care was taken in reproduce accurately the same experimental conditions, an intrinsic variability of the signals was observed when measuring different batches from the same cells. While the major spectral characteristics were preserved comparing samples with equivalent number of cells, the spectral intensities could vary from sample to sample. To give an idea, in Figure 12 we compare the AF spectra of three virtually identical batches of normal and SCC cells samples excited at the different wavelengths. Although the intensity variations can be quite considerable from batch to batch, comparing the normal and SCC signals within the same batch at a given excitation wavelength, it can be observed that SCC cells are in general less emitting than normal cells, at all emission wavelengths. Interestingly, above 400 nm of excitation wavelength, the adopted linear interferential filter is not capable to cut completely the frequency of the excitation radiation and some degree of backscattering is observed as peaks appearing at 405, 470, and 533 nm in Figure 12D–F, respectively. Although the analysis of the backscattered radiation is not the objective of the present work, it can be seen that the backscattering signal within the same batch in general also reduces for SCC cells compared to normal ones.

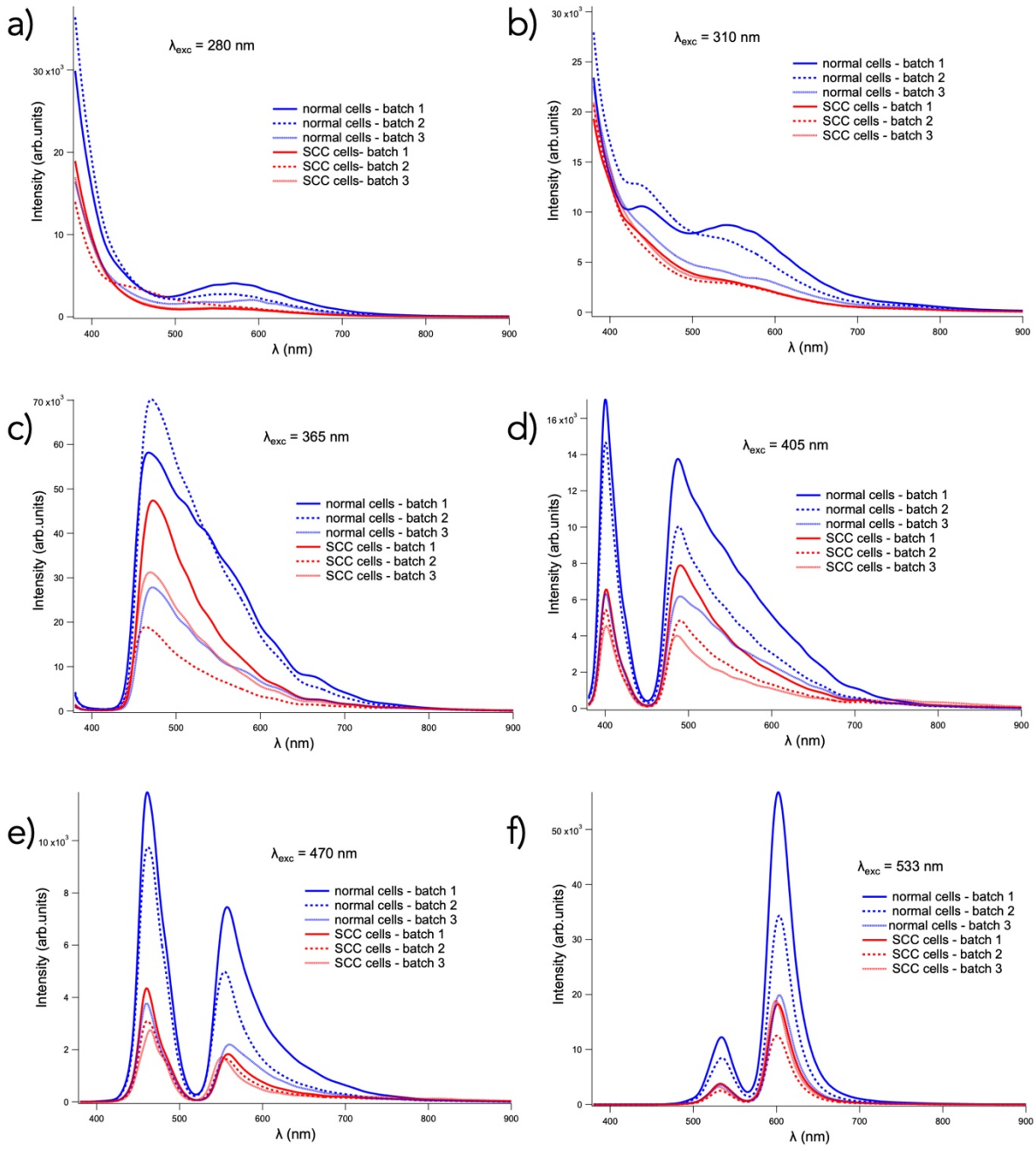

FIGURE 12. AF spectra taken at different excitation wavelengths on three batches (each batch is measured in the same day and under identical experimental conditions) of normal and SCC cultivated cells. All batches refer to 5 million cultivated cells.

In spite of the intrinsic variability, an overall distinctive behavior of normal and neoplastic cells is observed. In Figure 13A the most representative spectra are reported, referred to 5 million cultivated cells, both for normal and SSC keratinocytes (batch 1 of Figure 12). In this case, the backscattering contribution in the spectra taken at $\lambda_{exc} > 400$ nm has been removed, to highlight only AF emission. Normal cells show well defined features which appear more distinct when excited in the UV spectral range (λ_{exc} = 280, 310, and 365 nm). The line shape results progressively less structured as long as the excitation energy decreases (the wavelength increases). In all investigated cases and for all excitation wavelengths the SCC cells present a drastic reduction of AF in all regions with respect to the normal cells. The spectral features are also less defined.

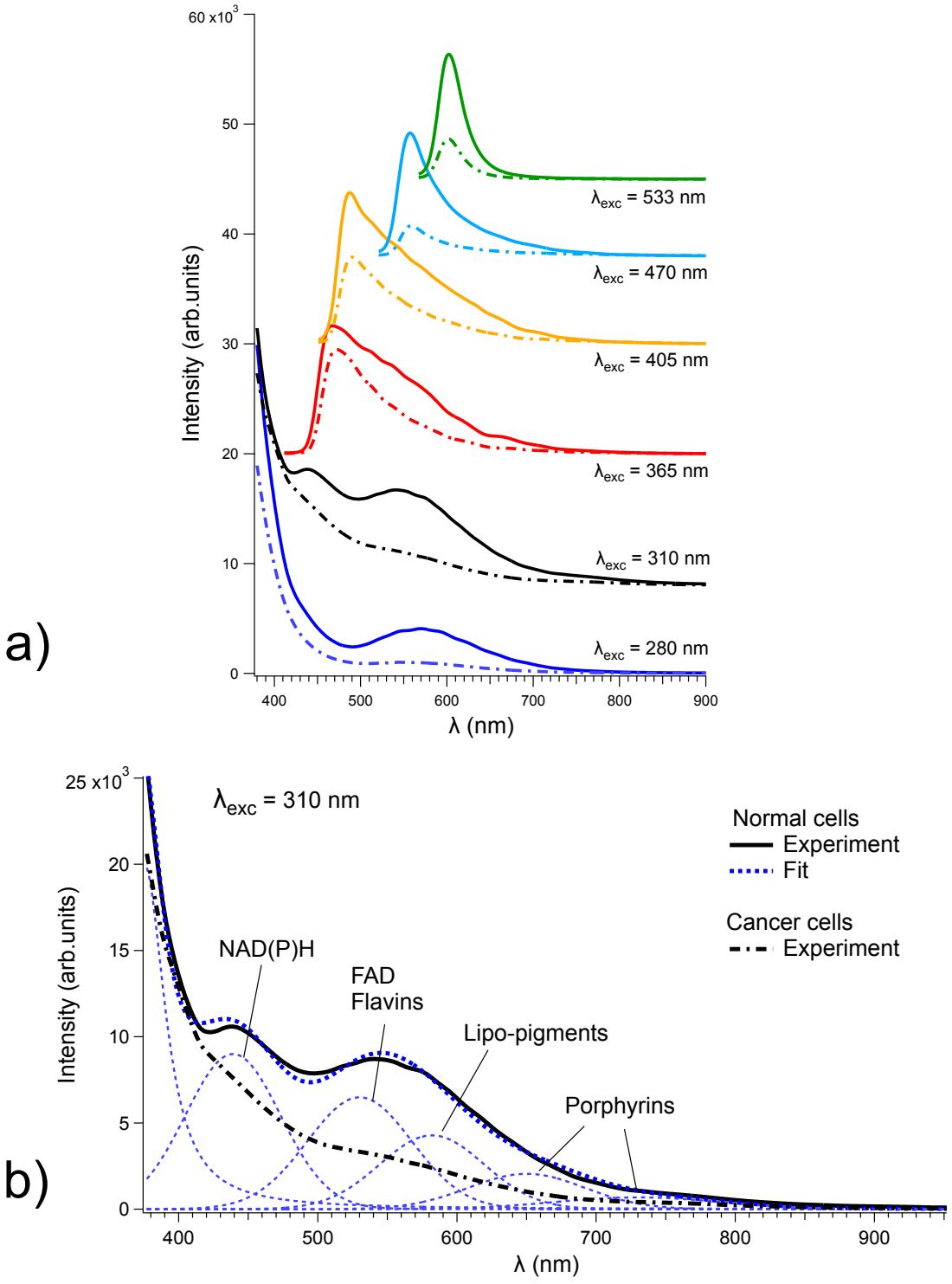

Figure. 13 (A) AF spectra as obtained at increasing excitation wavelengths. Continuous lines refer to normal cells and broken lines to NMSC (SCC) cells. (B) The fluorescence spectrum taken with λ_{exc} = 310 nm is shown, together with a best-fit decomposition of features using Gaussian profiles.

In Figure 13B the AF spectrum excited with photons at λ_{exc} = 310 nm, where spectral features appear more evident, has been decomposed with multiple Gaussian peaks in a least-squares fitting. Major contributions in normal cells can be associated to

characteristic luminescence from coenzymes nicotinamide adenine dinucleotide (phosphate) NAD(P)H, centered at about 440 nm, and flavin-adenin dinucleotide (FAD), at about 530 nm, which can be influenced by metabolic alterations [9,47,50,42]; higher wavelength structures can be associated to lipo-pigments, with maximum at 580 nm, and to porphyrins, at 650 nm and above 700 nm[62]. It is important to notice that all contributions are strongly depressed in the cancerous cells. This is in general agreement with observations also made in vivo [52,60,63,51]. FAD and NAD(P)H are metabolic coenzymes involved in the electron transport chain which are very sensitive to neoplastic alterations[49]. Their luminescence reduction in cancer cells is compatible with a change in the coenzymes redox state. While NAD(P)H is luminescent in the reduced state, flavins are luminescent in the oxidized state. The conversion of FAD to its reduced form has been previously reported during cancer progression in vivo[42], which results in luminescence reduction. On the other hand, NAD(P)H oxidation typically occurs in neoplastic cells with increased metabolism, due to its involvement in ATP and energy production[63,49]. This also contributes to the reduction of the luminescence. Regarding the signal of porphyrins, the decrease observed in this work seems to contrast the observations made in vivo, where an increase was sometimes measured[62]. This effect could be related to the more complex scenario that is present in skin tissues in vivo, where more components contribute to the luminescence. The role of blood drainage in skin tissues for example could play a fundamental role in this respect[62]. The decomposition of the spectra acquired at the other excitation wavelengths, or for SCC cells, is not shown here, since these spectra appear generally less structured compared to those of the normal cells excited with UV light. This may be related to the fact that UV radiation is more efficient in the excitation of the luminescent chromophores[63,47,64,50]. Although, we are not interested here in the relative intensities of the different components recorded at the different excitation wavelengths. Instead, the decomposition of Figure 13B is mostly informative on the main chromophore species contributing to the signals in the different spectral regions

and, indeed, all spectra taken at higher wavelength than 310 nm present broad emission in intervals covered by these chromophores.

The spectra shown in Figures 12 and 13 were obtained by separating the cells from the saline solution, so to increase the density of emitters in the probed area of the impinging beam and therefore increase the luminescence. To validate the results, further luminescence spectra were also taken with the cells still in saline solution, exploiting the experimental setup shown in Figure 11b.

AF spectra acquired from the cells in saline solution are reported in Figure 14. Although the overall luminescence signal is much lower with respect to the spectra of Figures 12 and 13 at all the probed excitation wavelengths, the same general trend is confirmed. At all excitation energies, the luminescence of the normal cells is always stronger than the pathological ones. Some excitation photons (i.e., at λ_{exc} = 365 and 405 nm) seem to induce a stronger luminescence intensity in the normal cells in the AF spectral region around 500 nm with respect to the other used photons, but this would need further confirmation and it is not the subject of the present study. Although attenuated by the linear interferential filter, some amount of scattered light, labeled “S” in Figure 14, is observed for λ_{exc} above 400 nm. It can be noticed that again the scattered light from normal cell is much higher than the pathological counterparts. The augmented scattering in normal cells might -at least partially- be related to the size as well as to the refractive index of the cells and their constituting elements[65]. However, these specific data are only preliminary results, that deserve further studies to be confirmed. On the other hand, this clear behavior could also be used to recognize normal versus pathological cells.

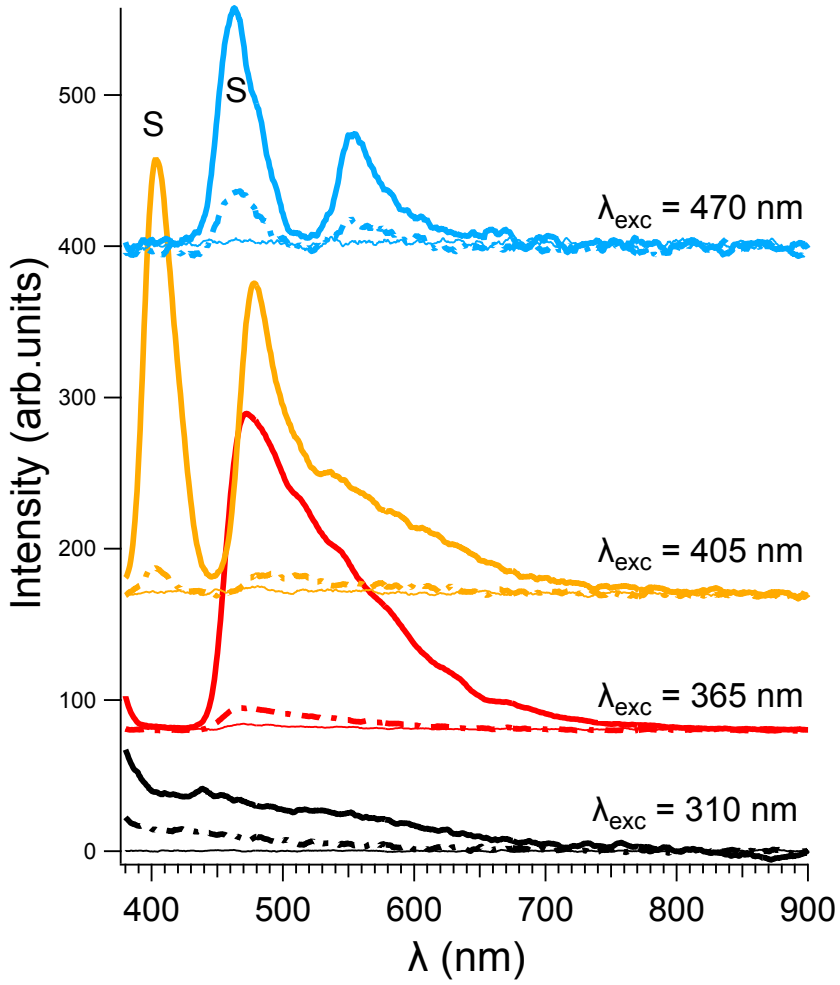

Figure. 14 Luminescence spectra acquired on cells suspended in saline solution. Continuous lines refer to normal cells and broken lines to SSC cells. The signal backgrounds, obtained with no cells in the physiological solution, are also reported as a thin continuous line. Labels "S" refers to scattered radiation of the excitation beam.

Last but not least, absorption experiments in transmission have been performed on a continuous and uniform layer of normal and SSC cells supported (grown) on a plastic Petri dish at comparable cell density. The results are shown in Figure 15.

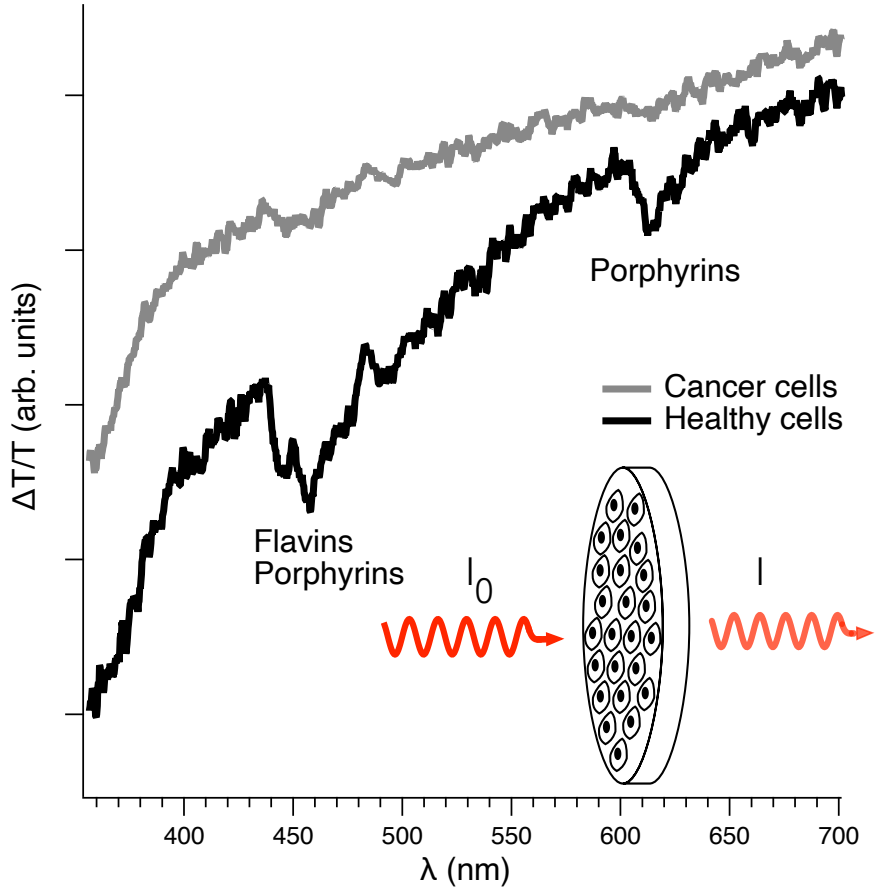

Figure. 15 ΔT/T spectra acquired on normal and cancer cells at comparable cell density. ΔT/T = (TPetri + cells – TPetri)/TPetri. A scheme of the transmission experiment is shown in the inset. T refers to the measure of the ratio between the beam intensity I after passing the sample and the I0 intensity (with no sample), as a function of the wavelength.

To highlight the contribution of the absorption of the cells, the spectra are shown in ΔT/T mode, that is subtracting the transmission TPetri of the clean Petri from the transmission TPetri + cells of the cells + Petri and dividing by the transmission of the clean Petri. Again, in Figure 15 the cells show a distinctive behavior: in particular the control cells present definite absorption features that can be related to flavins and porphyrins[47,50] that are almost absent, or strongly depressed, in SSC cells. Moreover, the differential transmission of normal cells in the region 500–600 nm and below 400 nm shows a slightly lower intensity, which can be related to a generalized higher absorption with respect to SCC cells, even if also an enhanced scattering could contribute.These findings support further the results of luminescence discussed

above, claiming for a reduction of NAD(P)H, FAD and flavins/porphyrins contribution in the cancerous cells.

Multivariate analysis of AF spectra

The above reported results seem to indicate a distinctive behavior of normal versus pathological cells that is relatively independent of the excitation wavelength. But since the AF spectra are indeed affected by some level of intrinsic variability, as noted above, we adopted an approach based on multivariate analysis to address the possibility to distinguish unambiguously solely from the luminescence signals normal cells from pathological cells. To this aim, the AF spectra acquired using the instrumental setup depicted in Figure 11a (cells deposited on Petri dishes) were considered, since it led to overall luminescence signals much higher than those recorded on cells suspension. The whole set of AF spectra is reported in Figure 16, colored both according to the different excitation wavelengths (Figure 16a), and according to the class of samples (Figure 16b). As it was clearly expected, the spectral signatures differ mainly due to the different excitation wavelengths. It should be noted that the spectra presented in Figure 16 also include some contributions (peaks) due to the backscattered excitation wavelengths, whenever these fall in the spectral range measured by the spectrometer (348–1132 nm) and the interferential, high pass, linear variable filter is not able to completely suppress them. These peaks were in any case included in the multivariate analysis, since they also seem informative of the nature of the cells, as noted above.

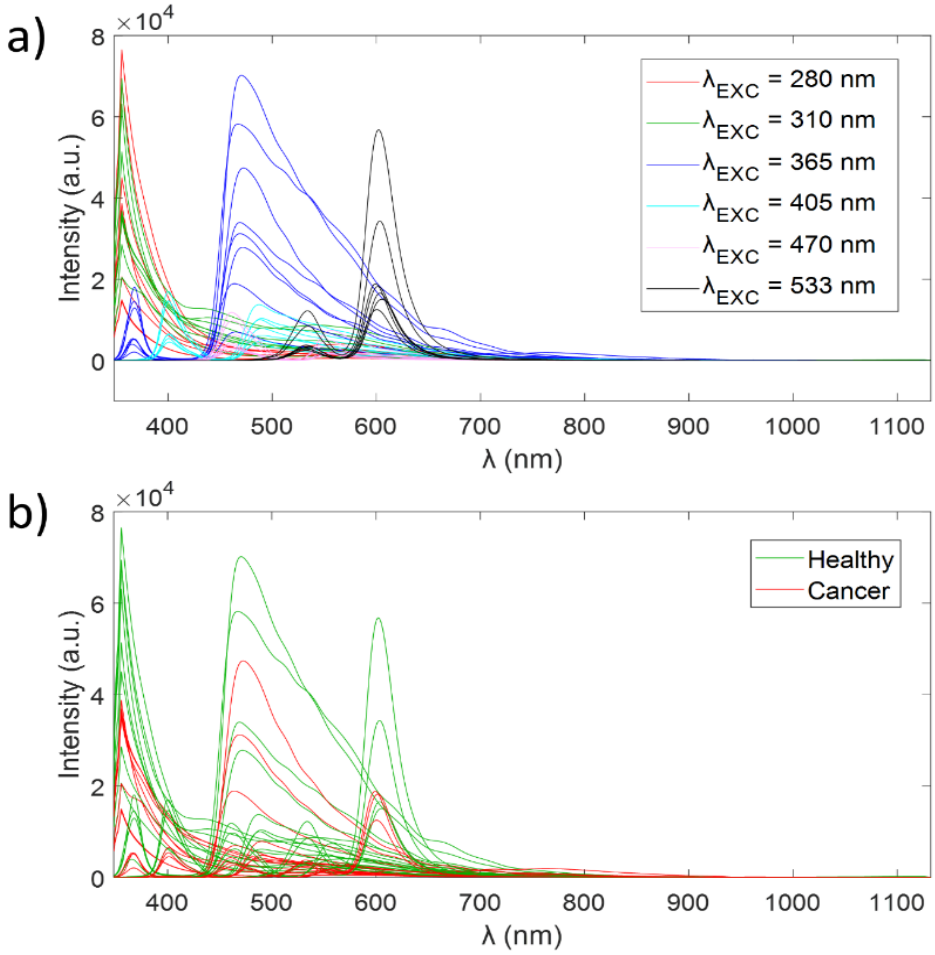

Figure. 16 Dataset of AF spectra subjected to multivariate analysis, colored according to the different excitation wavelength (a) and according to the class of samples (b).

PCA of the AF spectra from single excitation wavelengths

Firstly, an exploratory data analysis was conducted by calculating separate PCA models on the groups of spectra measured at each excitation wavelength, in order to further verify that, based on an unsupervised approach, the patterns of spectra measured at a given excitation wavelength on healthy cells differ from those measured on cancer cells. As an example, Figure 17 reports the PC1-PC2, PC1-PC3 score and loading plots of the PCA models calculated on the mean centered spectra measured at λ_{exc} =280nm, $\lambda_{exc=}$ 310 nm, λ_{exc}= 365nm, λ_{exc} =405nm, λ_{exc} =470nm and at λ_{exc} = 533 nm.

Figure. 17 PC1-PC2, PC1 -PC3 score plot (left column) and loading plot (right column) of the AF spectra measured at λexc = 280, 310, 365, 405, 470, 533 nm

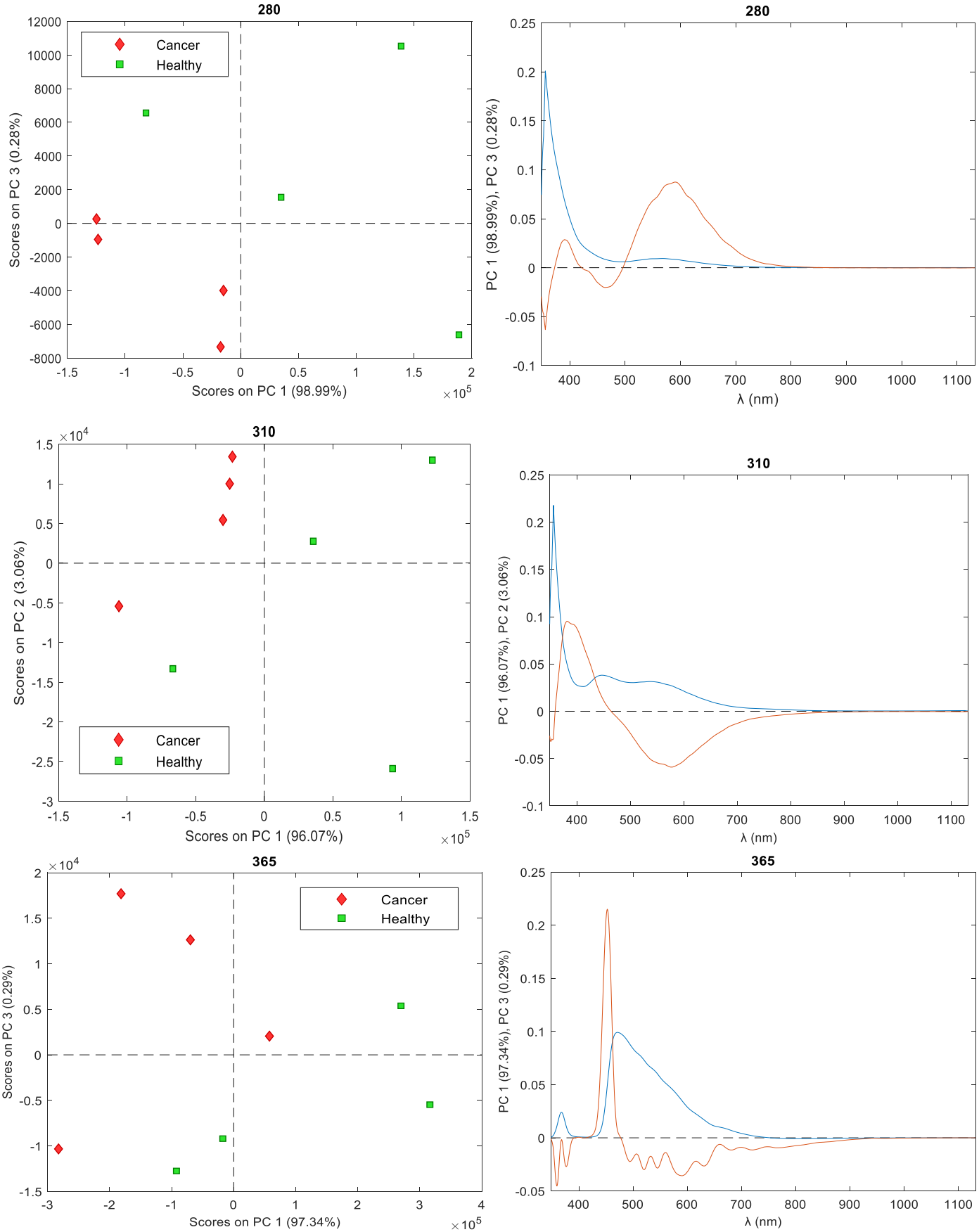

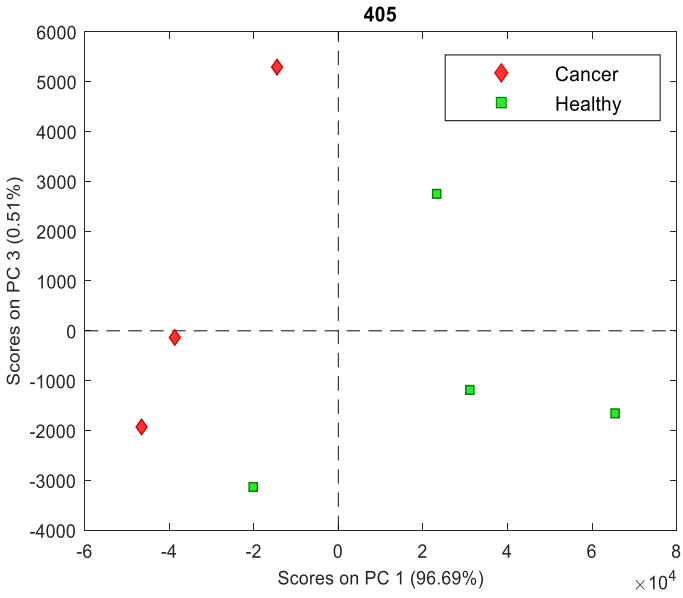
405
Cancer
Healthy
Scores on PC 3 (0.51%)
Scores on PC 1 (96.69%)
×10^4

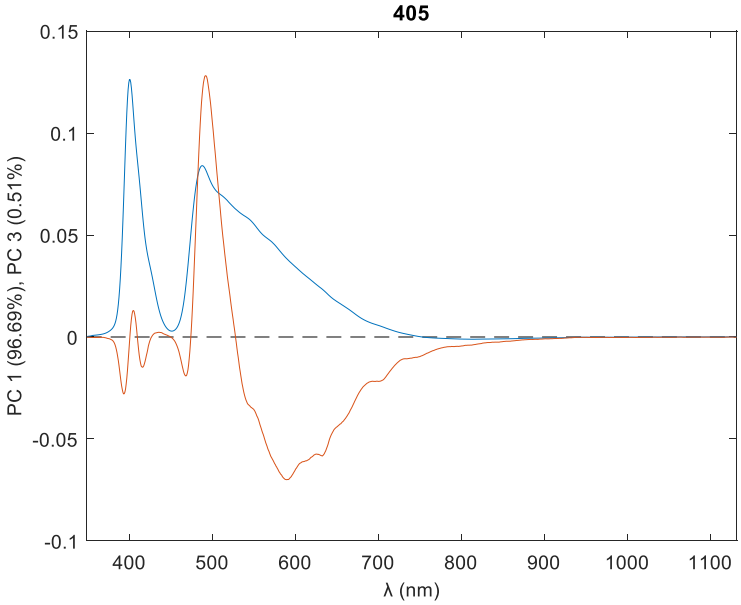
405
PC 1 (96.69%), PC 3 (0.51%)
λ (nm)

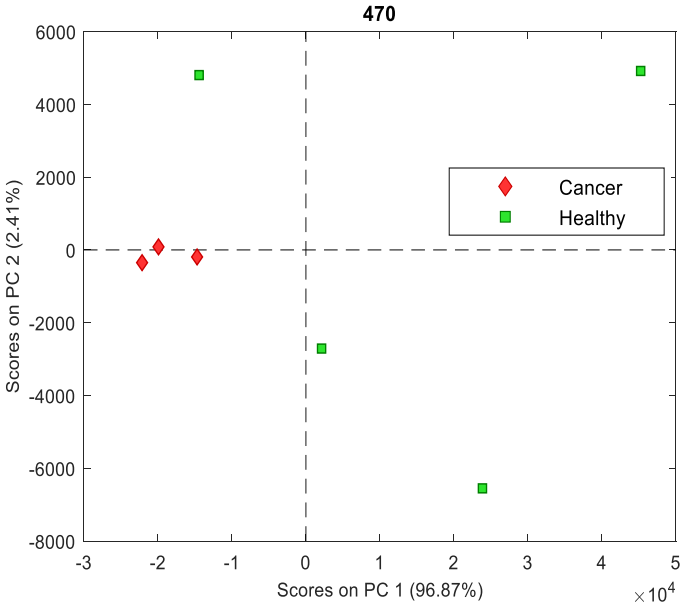
470
Cancer
Healthy
Scores on PC 2 (2.41%)
Scores on PC 1 (96.87%)
×10^4

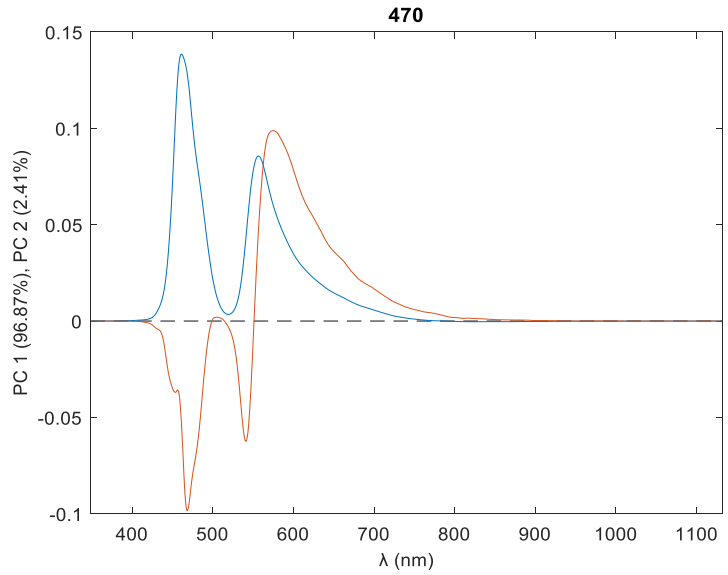
470
PC 1 (96.87%), PC 2 (2.41%)
λ (nm)

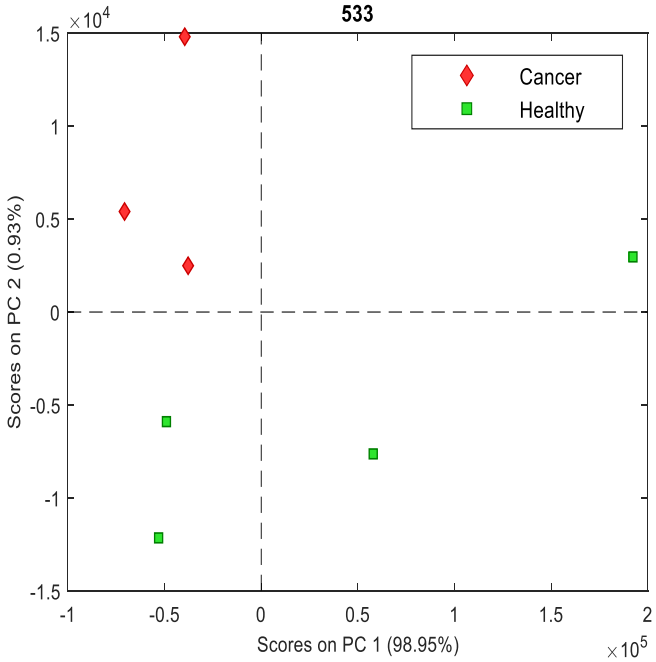
533
×10^4
Cancer
Healthy
Scores on PC 2 (0.93%)
Scores on PC 1 (98.95%)
×10^5

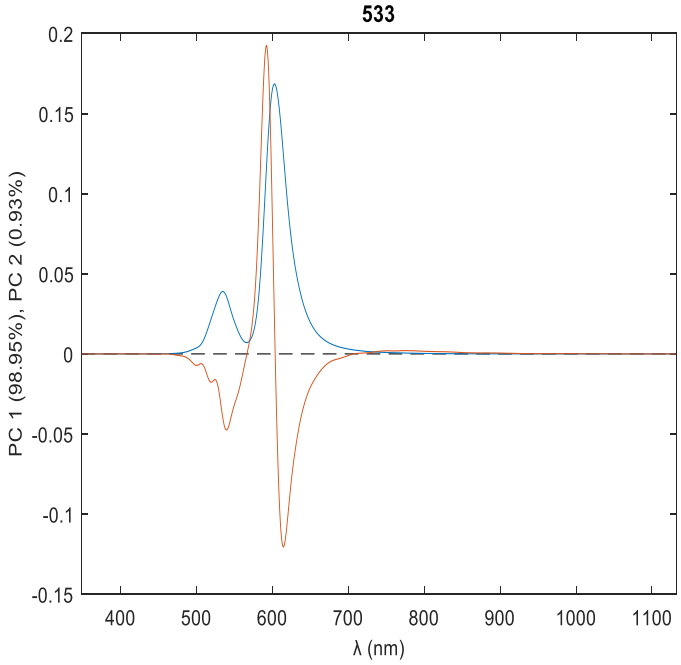
533
PC 1 (98.95%), PC 2 (0.93%)
λ (nm)

Both the PC1-PC2 score plots (Figure 17 left column for λ_{exc} = 310 and 533 nm, respectively) show that the AF signals acquired on the NMSC cells are separate from the healthy cells. Moreover, it can be observed that the AF signals of healthy cells are more spread with respect to those measured on NMSC cells, which indicates that the signals measured on healthy cells show a greater variability with respect to those measured on NMSC cells. The corresponding loading plots reported in Figure 17 (right column) show the spectral regions that mainly contribute to the separation between the two groups. A similar behavior was observed, either in the PC1-PC2 or in the PC1-PC3 space, for all the excitation wavelengths. In general, excluding the lower wavelength spectral regions, where contributions from some of the excitation wavelengths are present in some cases, the region common to all the AF spectra where the PCA loading vectors showed the highest absolute values was the one between 550 and 850 nm. This is a relevant region also for applications, since for measurements in vivo, this offers the opportunity to use, for excitation, photons in the visible range, which can be more practical. We stress, in any case, that the emission region above 550 nm appears to be the informative one for all datasets, including those obtained with excitation in the UV.

PLS-DA classification of the AF spectra

Since for each separate group of spectra measured at a given excitation wavelength PCA confirmed the difference between the patterns of healthy and cancer cells, particular in the region between 550 and 850 nm and given that this difference seemed relatively independent of the excitation wavelength, multivariate classification was then performed to verify these findings, regardless of the specific excitation wavelengths. To this aim, the region between 550 and 850 nm was therefore considered for the calculation of two PLS-DA models, one on mean centered variables and one on auto scaled variables, and considering the whole set of spectra as described in section "*PLS-DA classification models on the whole dataset*"

TABLE 15 Results of the PLS-DA models calculated on the whole dataset of AF spectra considering the 550–850 nm range

Preprocessing method	**LVs**	**$SENS_{CAL}$**	**$SPEC_{CAL}$**	**EFF_{CAL}**	**$SENS_{CV}$**	**$SPEC_{CV}$**	**EFF_{CV}**	**$SENS_{PRED}$**	**$SPEC_{PRED}$**	**EFF_{PRED}**
Mean center	3	100.0 %	68.8 %	82.9 %	93.2 %	65.3 %	78.0 %	100.0 %	87.5 %	93.5 %
Autoscale	4	100.0 %	75.0 %	86.6 %	95.0 %	66.9 %	79.7 %	100.0 %	87.5 %	93.5 %

Note: The Sensitivity (SENS) and Specificity (SPEC) values are referred to the class of the cancer (NMSC) cells, while classification efficiency (EFF) is the geometric mean of SENS and SPEC.

Both the classification models showed satisfactory performances. Slightly better values were obtained in calibration and in cross validation with the model calculated considering the auto scaled variables, while the same results were obtained for the prediction of the test set samples, where only one healthy sample measured at λ_{exc} = 470 nm was misclassified in both the models. The SENS values, indicating the ability to correctly identify the NMSC samples, were always very high, while the SPEC ones

were always lower, indicating that the largest part of misclassifications were due to the incorrect attributions of healthy samples to the NMSC class.

Interestingly, both the PLS-DA models showed very similar values of the variable importance in projection (VIP) scores[66,67], as reported in Figure 18. The VIP scores allow to estimate the importance of each variable used in a PLS model: the variables with VIP values higher than a fixed limit (usually set equal to 1) are considered significant for the model. For both the models, the VIP scores suggest that the spectral region significantly contributing to the discrimination between NMSC and healthy cells is between 550 and 670 nm. The two peaks, centered at about 590 and 650 nm, are very close to the peaks of lipo-pigments (580 nm) and of porphyrins (650 nm), respectively, as it was previously discussed in the comments to Figure 13B. Furthermore, the high values between 550 and 570 nm could be ascribable to the peak of FAD, which has a maximum centered at about 530 nm.

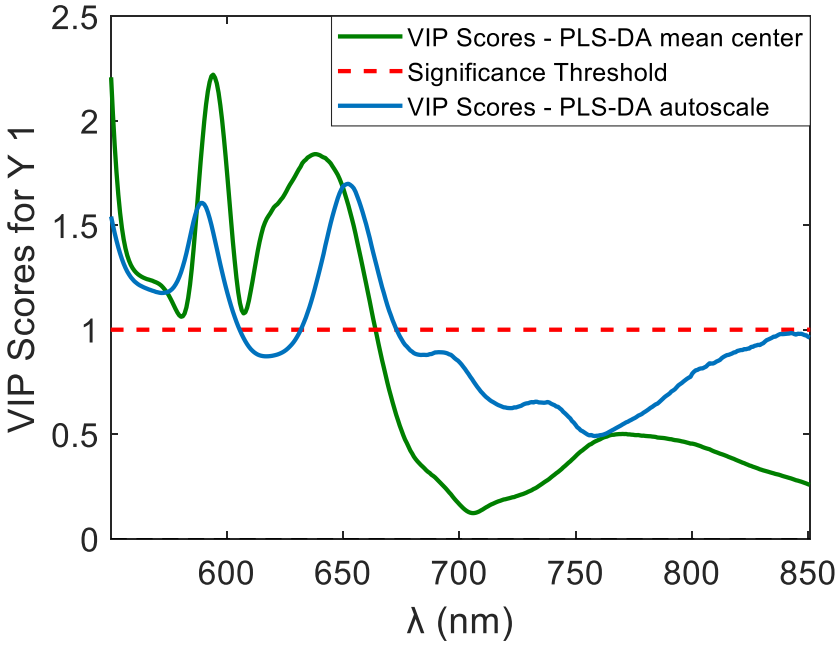

Figure. 18 VIP scores of the PLS-DA models calculated on mean centered variables (green line) and on auto scaled variables (blue line)

Finally, the statistical significance of the best performing classification model, that is, of the PLS-DA model calculated on the auto scaled variables, was further checked by means of a permutation test. Figure 19 shows the results of the permutation test, where the EFF values of the correct model (full squares) and of the permutations (empty circles) are reported as a function of the percentage of matching between the correct class assignation and the randomly shuffled one.

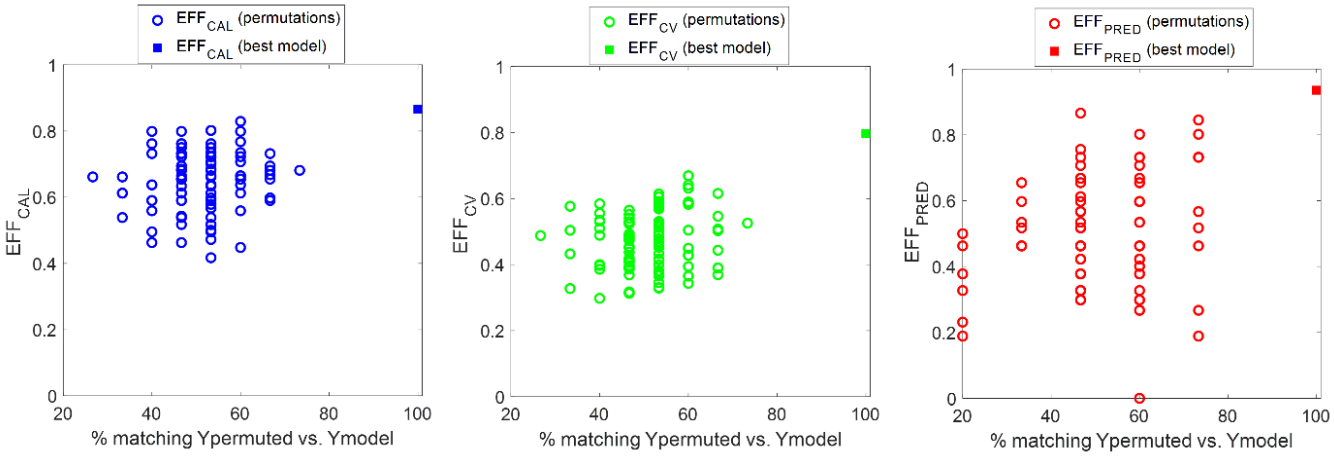

Figure. 19 Comparison of the classification efficiency values obtained for the best PLS-DA model (full squares) with the corresponding values obtained with the permutation test (empty circles). The plot on the left reports the EFFCAL values (blue); the central plot reports the EFFCV values (green), and the plot on the left reports the EFFPRED values (red)

To evaluate whether the EFF values obtained for the correct model (i.e., the best PLS-DA model) were statistically significant, they were compared with the distribution of the corresponding EFF values from permutations, using a one-tailed t test.

Table 16 reports the EFF values obtained with the best PLS-DA model, the mean (m) and standard deviation (s) of the EFF values obtained with the permutation test, and the corresponding results of the one-tailed t tests. The results confirm that the significance of the EFF values obtained with the best PLS-DA model is much lower than 0.05, that is, that the good performance of the selected classification model is not due to chance

Table 16 Results of the one-tailed t test performed on the EFFCAL, EFFCV, and EFFPRED values reported in Figure 18

	Best model	Permutations		One tailed t-test		
		m	s	t_{CRIT}*	t_{CALC}	$P(t_{CALC})$
EFF_{CAL}	0.866	0.646	0.089	1.660	2.459	7.84×10^{-3}
EFF_{CV}	0.797	0.472	0.086	1.660	3.761	1.43×10^{-4}
EFF_{PRED}	0.935	0.488	0.160	1.660	2.789	3.17×10^{-3}

** P = 0.05; df = 99*

5 Comparative in-vitro autofluorescence study from healthy cells to skin tumor cells at different excitation wavelengths

5.1 Introduction

Throughout the process of cancerization, cells undergo structural alterations that influence AF emission patterns. Our ex vivo study illustrated the potential to distinguish healthy from cancerous tissue based on AF variations.[68] The modifications in fluorophore metabolism, distribution, and concentration in cancerous tissue result in a hypofluorescent appearance in AF emission spectra.

Building upon our previous work,[60] we transitioned from ex vivo to in vitro evaluation to ascertain whether disparities between cancerous and healthy keratinocytes could be identified. SCC cells exhibited a hypofluorescent profile in contrast to healthy cells, underscoring the utility of AF in detecting differences not only within the complex milieu of tissue but also at the single-cell level.

In this study, we aimed to reaffirm our previous findings by adjusting certain parameters. In former studies, we used a tumor cell line derived from tongue SCC, and pool keratinocytes obtained from cutaneous discarded tissue. In order to avoid possible biases due to the heterogeneity of cell sources, we decided to employ cutaneous SCC cells and keratinocytes from cell lines in this project.

5.2 Materials and Methods

A-431 SCC cell line was used for in vitro evaluation of the behavior of tumoral cells from SCC. Primary human epidermal keratinocytes - HEKa cell line (PCS-200-011)- were used as healthy controls. Cells were HPVneg p53+.

Cells were seeded into culture flasks with a surface area of 75 cm^2 and recovered when the culture has reached approximately 70%-80% of confluence. Cell viability was assessed using Trypan blue assay. To enhance the luminescence signal from the cells and prevent any signal interference caused by the culture solution, autofluorescence (AF) was measured on cell pellets (2 million cells suspended in 20 µl). These pellets were subsequently placed on an appropriate support surface and special attention was given to promptly acquiring AF data after removing the cells from the solution to minimize any potential deterioration. Experiments were performed in triplicates.

The optical set up was the same used in previous experiments [68]. A tilt angle of 30° was used. Three different measurements were performed for each sample in three different regions of the pellet. Results were recorded as mean ± standard deviation. Five different excitation wavelengths were used, ranging from 280nm to 533nm. The experimental setup was described previously in Figure 11a which illustrates the arrangement used for luminescence measurements from the cell pellets.

5.4 Results and discussion

In Figure 20 the emission spectra are graphically represented at increasing excitation wavelengths; logarithmic scales have been used to emphasize differences. Peak regions were excluded. (Figure 20)

keratinocytes (h)/ tumour (t) – Autofluorescence

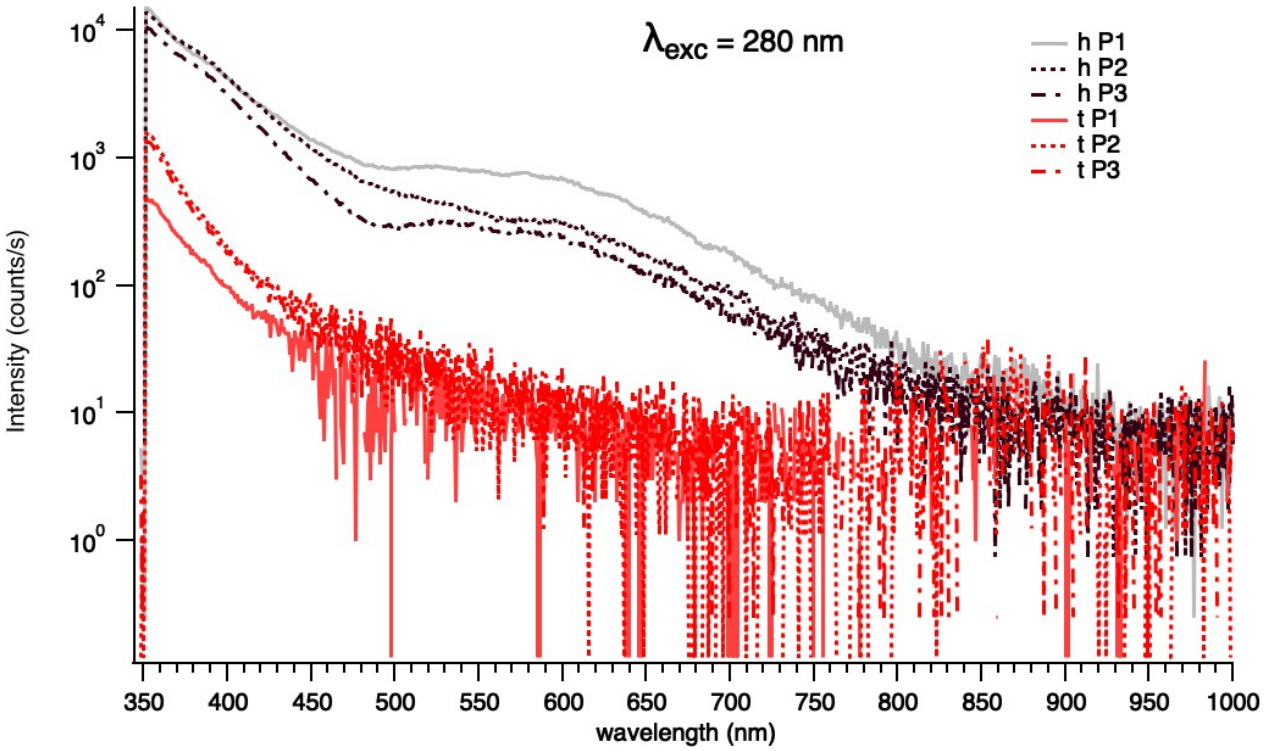

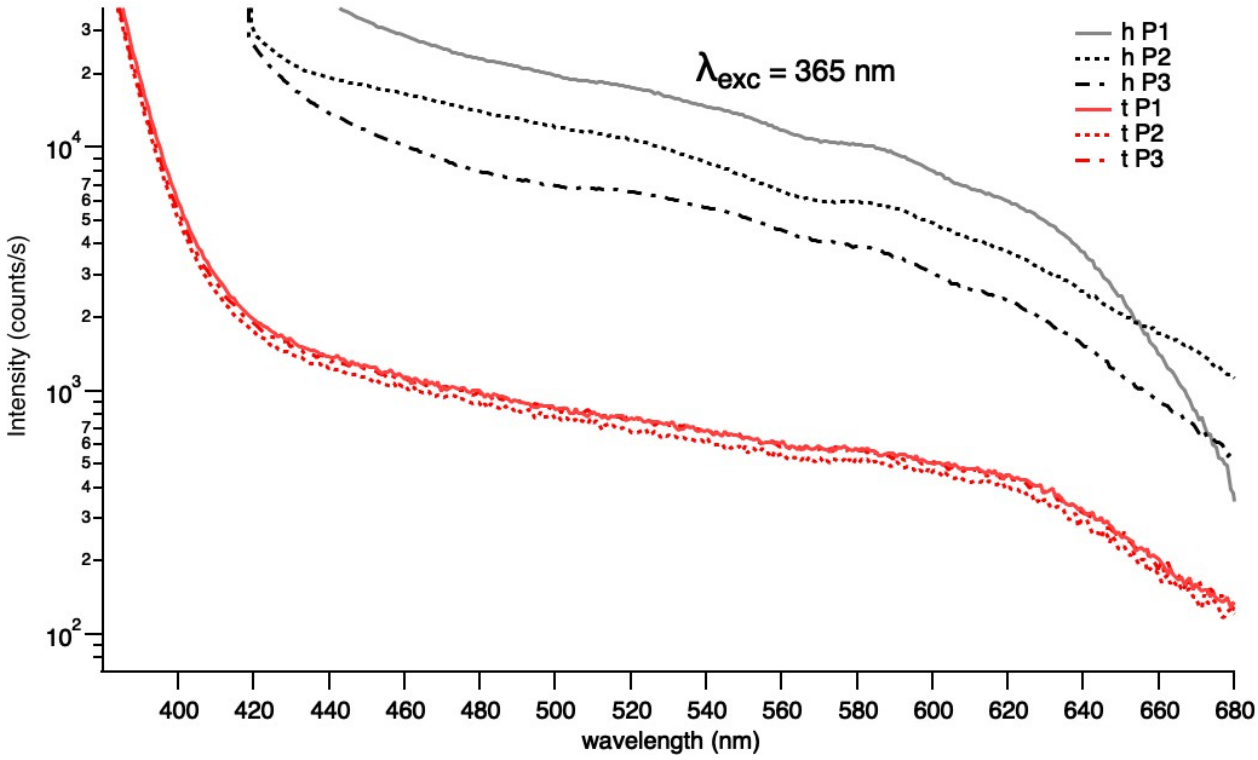
λexc = 365 nm
h P1
h P2
h P3
t P1
t P2
t P3
Intensity (counts/s)
wavelength (nm)

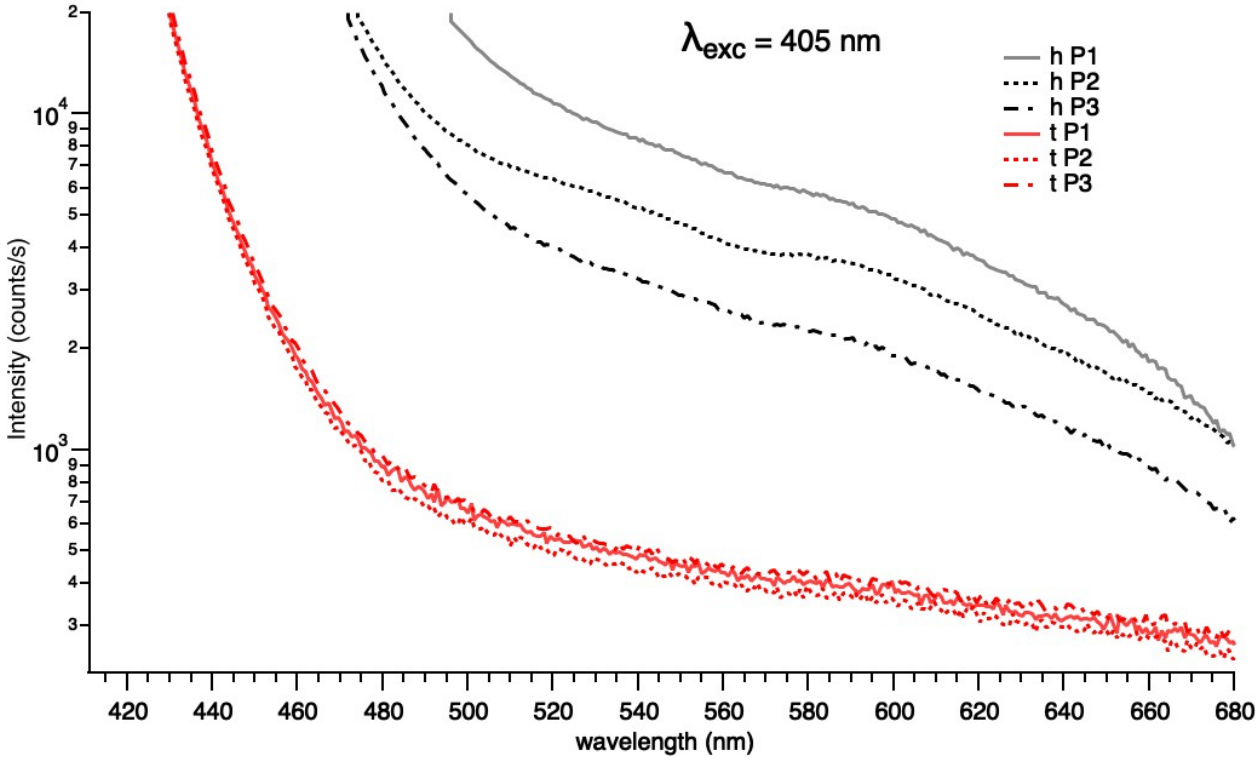
λexc = 405 nm
h P1
h P2
h P3
t P1
t P2
t P3
Intensity (counts/s)
wavelength (nm)

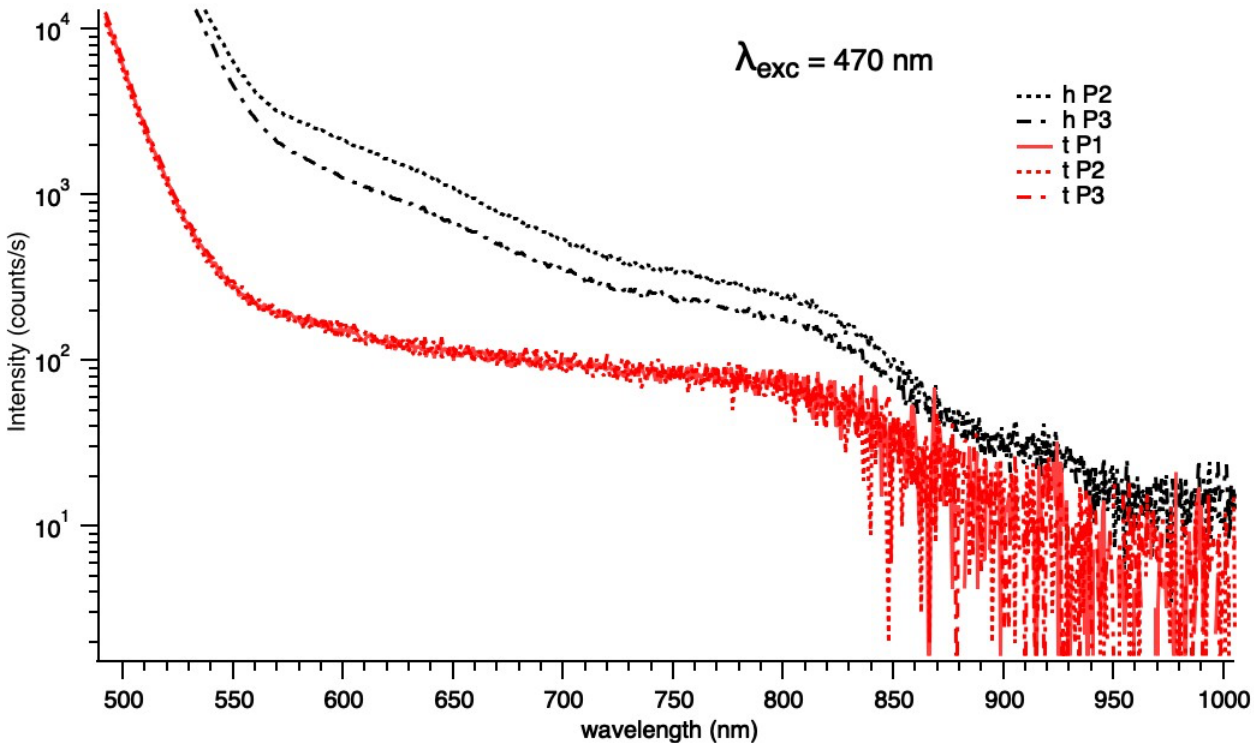

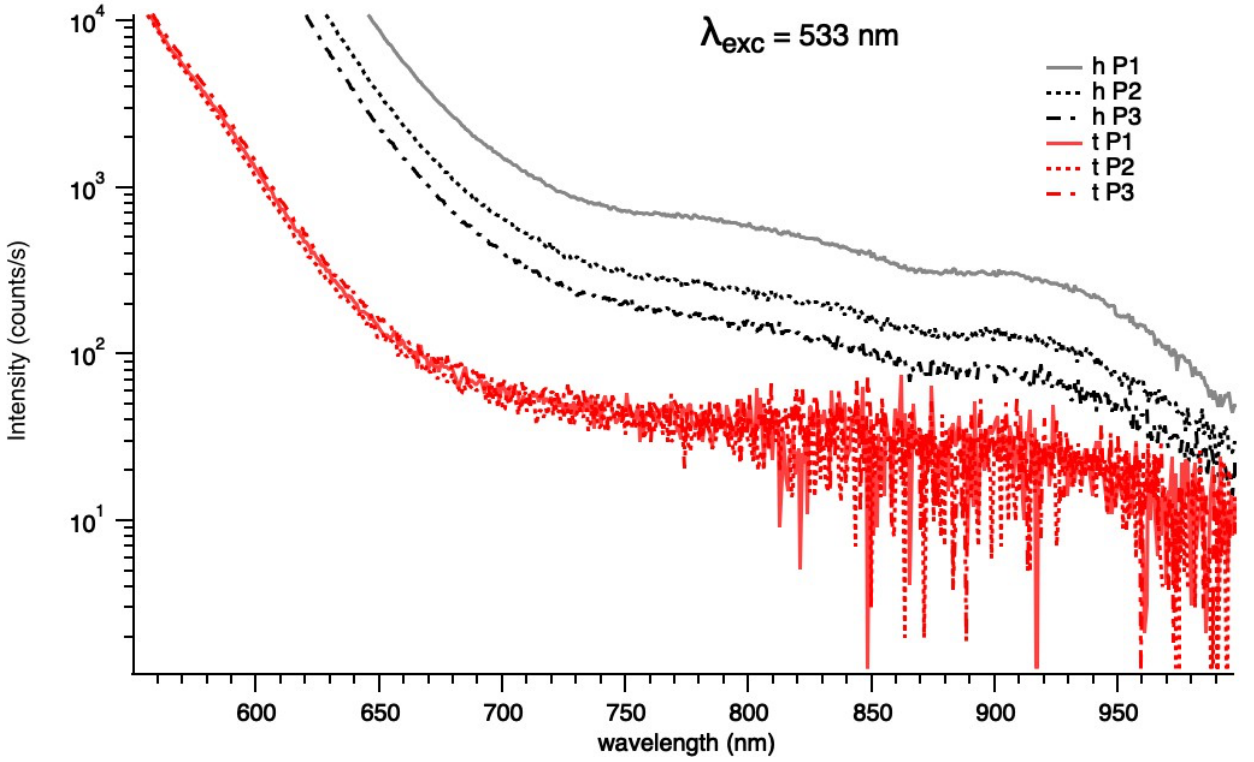

Figure 20 The figure describe the different aspect of the AF emission spectra at the different excitation wavelengths. In the y axis we put the intensity in logarithmic scale, in the x axis the different wavelengths. Grey colors with full and dotted lines represent the healthy keratinocytes in the different sampling points. In the red lines with dotted and full aspect, we can see the SCC tumors cells in the different sampling positions.(P1,P2,P3)

As shown above, healthy keratinocytes show higher AF compared SCC cancer cells in each spectral region.

The spectra are determined by the contribution of different fluorophores present in the cells. In particular we used the same excitation wavelength of our previous in-vitro study [68], to stimulate keratinocytes derived from healthy keratinocyte and SCC cell lines, to better define the reliability of our results.

In previous experiments, SCC cells were compared to three-donor pool keratinocytes obtained from the discarded tissue from surgical interventions. Therefore, internal variability was possibly related to the heterogeneity of the samples. On the contrary, cell lines represent a more standardized model. Moreover, we decided to set a pre-defined number of passages in culture (three) and a fixed volume of PBS for pellet dilution before AF measurements (2 million cells in 20 µl).

Furthermore, the A-431 SCC cell line is derived from skin SCC, while former data were obtained from tongue SCC, with possible biases due to site-specific expression of intracellular fluorophores.

As already mentioned, most of the AF in healthy cells is possibly linked to the presence of coenzymes such as nicotinamide adenine dinucleotide (phosphate) NAD(P)H, with a peak around 440 nm, and flavin-adenine dinucleotide (FAD), at approximately 530 nm.[9,8,69] These emissions are subject to influence by metabolic changes. Additionally, longer-wavelength emissions can be associated with lipo-pigments, peaking at around 580 nm, and porphyrins, which exhibit peaks at 650 nm and beyond 700 nm.[63,12] Weaker contribution of such fluorophores is detected in cancerous cells.[54] A possible explanation resides in the multiple changes that occur in the cancerization process in the intimate modification of the cell structure. These data confirm that the AF emission spectra from healthy and tumoral cells differ not only at a tissue- but also at a cell level.[68]

We also noticed some slight differences both between pool keratinocytes and HEK cell lines and between tongue and skin SCC.

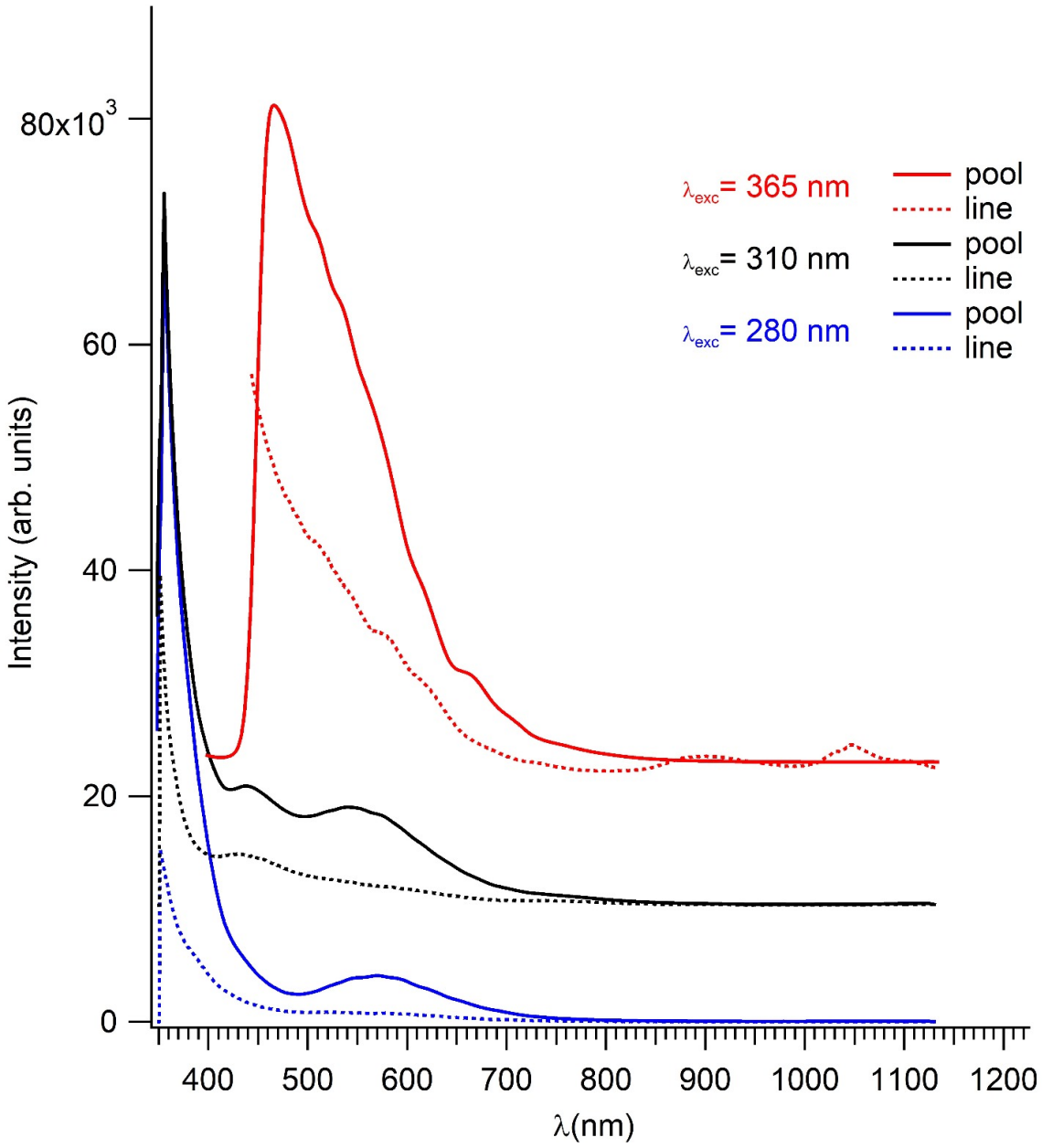

Figure 21 : the figure describe the comparison of the AF emission spectra among keratinocytes, taken from lines and taken from a pool of donor; here we show you the excitation from 280 to 365 nm where we can better observe the hypofluorescent aspect of the keratinocytes derived from cell lines.

As we shown in Figure 21, with excitation wavelengths ranging from 280nm to 365nm, the keratinocytes from cell lines demonstrated and hypofluorescent aspect respect the keratinocytes from pool of donor. This could have different explanations, such as the differences in terms of number of passages in culture, dilution of the cell suspension for AF measurements.

We used a mathematical algorithm known as “fitting” to decompose the curve, isolating the individual contributions of the fluorophores. This procedure enabled us to qualitatively analyse the emission spectra.

In each fitting graph, the initial region represented the starting excitation peak, the second corresponded to NADH at approximately 440 nm, the third delineated the FAD peak at 530 nm, lipopigments at 580 nm, and the fifth area indicated porphyrins at 650 nm.

Figure 22 illustrates how the fitting process revealed distinct contributions of NADH and FAD in both pool and line keratinocytes.

In particular, the emission spectrum of cell-line keratinocytes prominently displayed contributions from NADH and FAD, whereas pool keratinocytes primarily exhibited contributions from both NADH and lipopigments.

The properties of NADH and flavins already demonstrated a prominent role in AF based Optical biopsy. NADH fluoresces in its reduced state, while flavins fluoresce in the oxidized state. The emission properties of AF are closely tied to the bound/free condition of these coenzymes. These molecules play a crucial role in the fluorescence originating from cell cytoplasm, with their quantity and redox state intricately linked to their involvement in energetic metabolism, cellular oxidative defence, reductive biosynthesis, and signal transduction. The flavin-adenin dinucleotide (FAD), display an absorption/excitation and emission peaks occur around 440-450 nm and 525 nm, respectively. Additionally, the fluorescence emission from FAD is significantly influenced by the nature of the protein to which the prosthetic group is attached.

Besides the diffuse fluorescence emanating from NAD(P)H and flavins, there are occasionally observed intensely glowing particles attributed to lipofuscin or lipofuscin-like lipopigments within the cell cytoplasm.[70,9]The fluorescence of lipofuscin encompasses the yellow-reddish spectrum, with its spectral profile and emission intensity contingent upon the variations in composition (proteins, lipids, carotenoids), crosslinks, and oxidation state of these diverse compounds, as well as the aging process. Generally, lipofuscins constitute undigested remnants from phagocytosis and autophagy processes, accumulating as intracytoplasmic granules influenced by the physiological metabolic activity of the cell, the aging phenomenon, and the manifestation of disorders and pathologies resulting from oxidative stress.

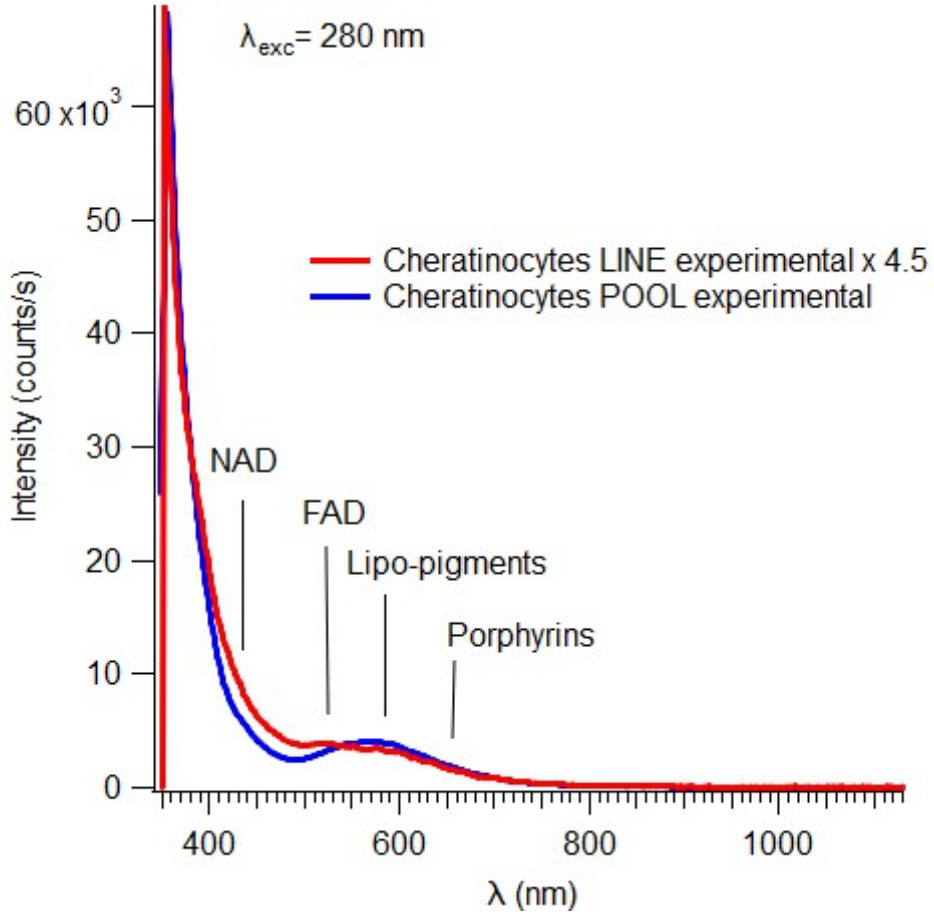

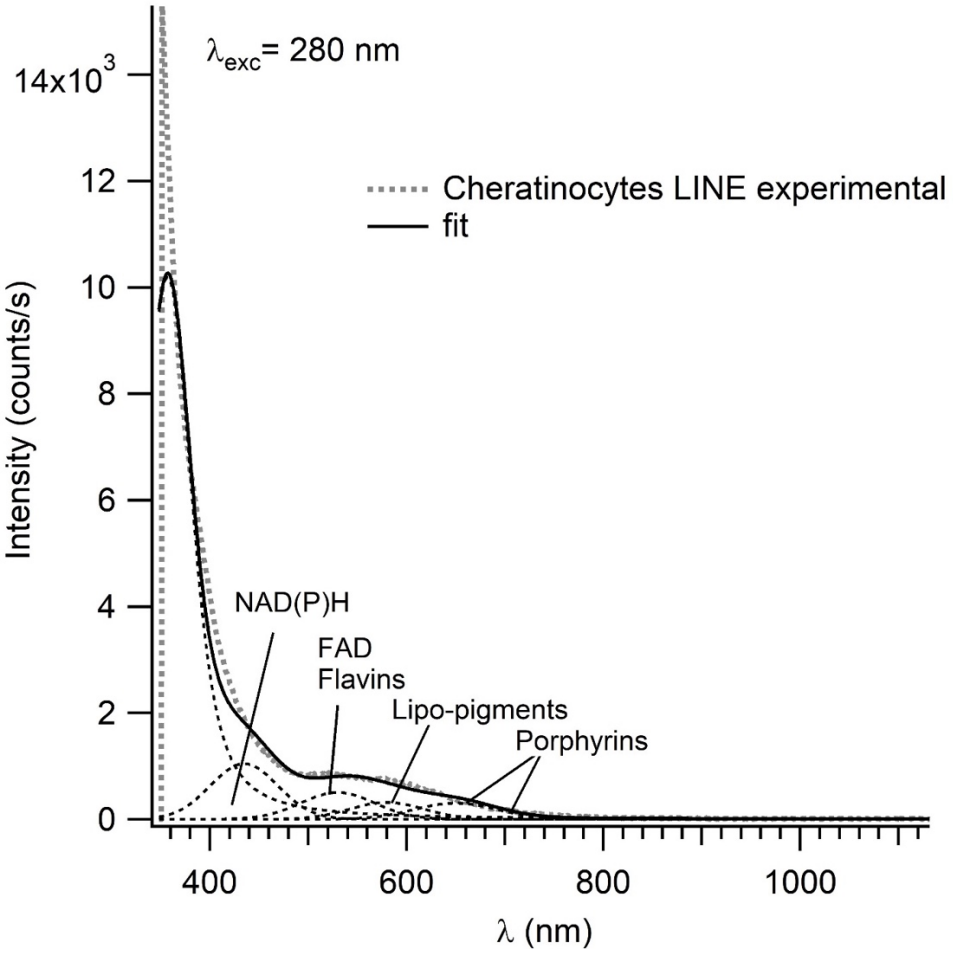
λexc= 280 nm
14x10^3
12
10
8
6
4
2
0
Intensity (counts/s)
Cheratinocytes LINE experimental
fit
NAD(P)H
FAD
Flavins
Lipo-pigments
Porphyrins
400
600
800
1000
λ (nm)

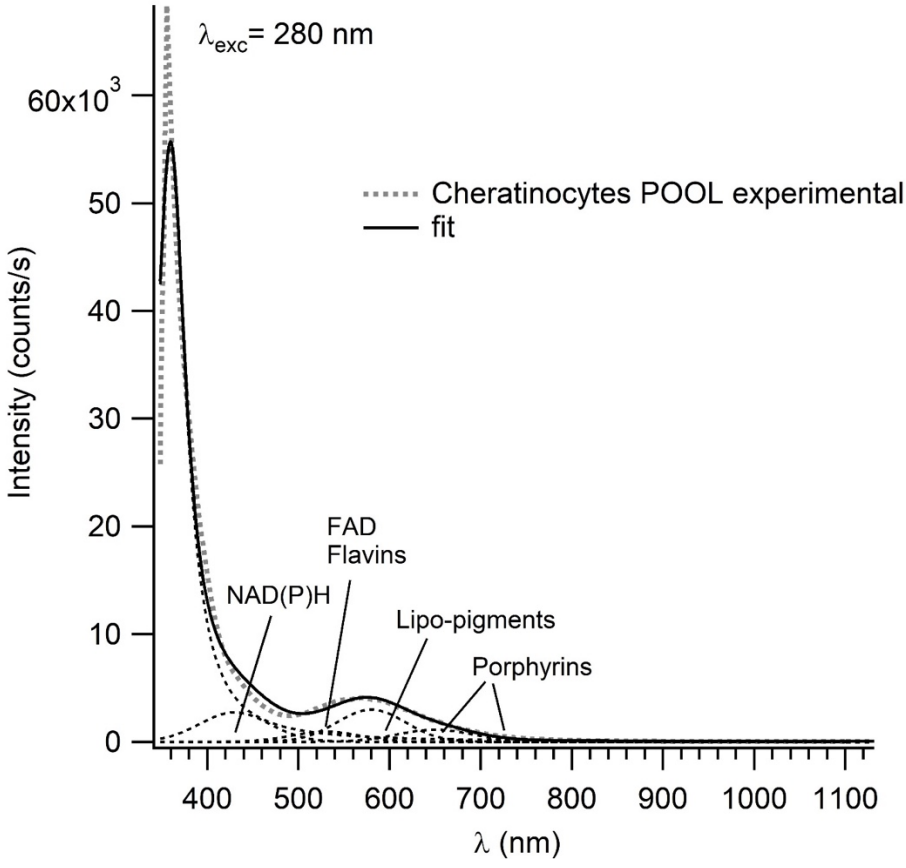
λexc= 280 nm
60x10^3
50
40
30
20
10
0
Intensity (counts/s)
Cheratinocytes POOL experimental
fit
FAD
Flavins
NAD(P)H
Lipo-pigments
Porphyrins
400
500
600
700
800
900
1000
1100
λ (nm)

Figure 22: **The fluorescence spectrum taken with λ_{exc} = 280nm is shown, together with a best-fit decomposition of features using Gaussian profiles of both keratinocytes from pool and lines.**

Through the fitting process, it became possible to demonstrate the distinct roles played by the predominant fluorophores in shaping the emission spectrum. As previously observed, NAD(P)H exhibited a signal higher than FAD and closely resembled lipopigments in the POOL. In the LINES, FAD made a more substantial contribution, accompanied by a significant presence of NAD(P)H and minimal lipopigments.

The inverse correlation between the differentiation degree in stem cells[71] and the abundance of lipofuscins/lipopigments suggests that the accumulation of these substances may result from the impact of reactive oxygen species on autophagocytosed mitochondria rather than normal physiological aging processes. Despite the POOL cells being derived from multiple donors and treated similarly to cell lines, the presence of abundant lipopigments may be associated with different cellular metabolism rather than the preceding differentiation.

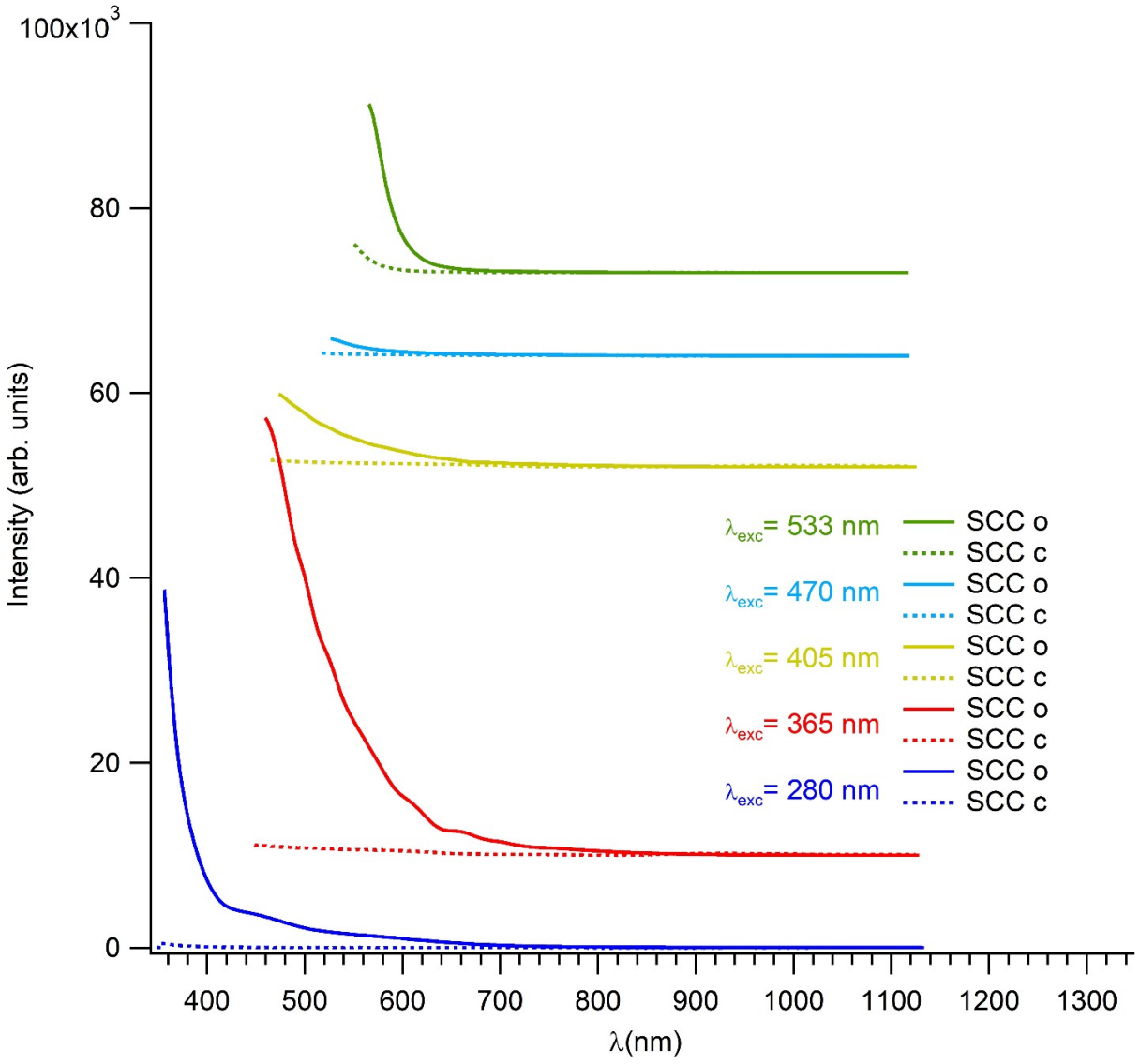

Figure 23: Here we can show the emission spectra of SCC from tongue (o)(full line)(UPCI:SCC154) cell line and SCC from skin cell line(c)(dotted line) (A-431 SCC) at different excitation wavelength. It is noticeable that SCC from tongue shows an hyperfluorescent aspect respect the skin SCC.

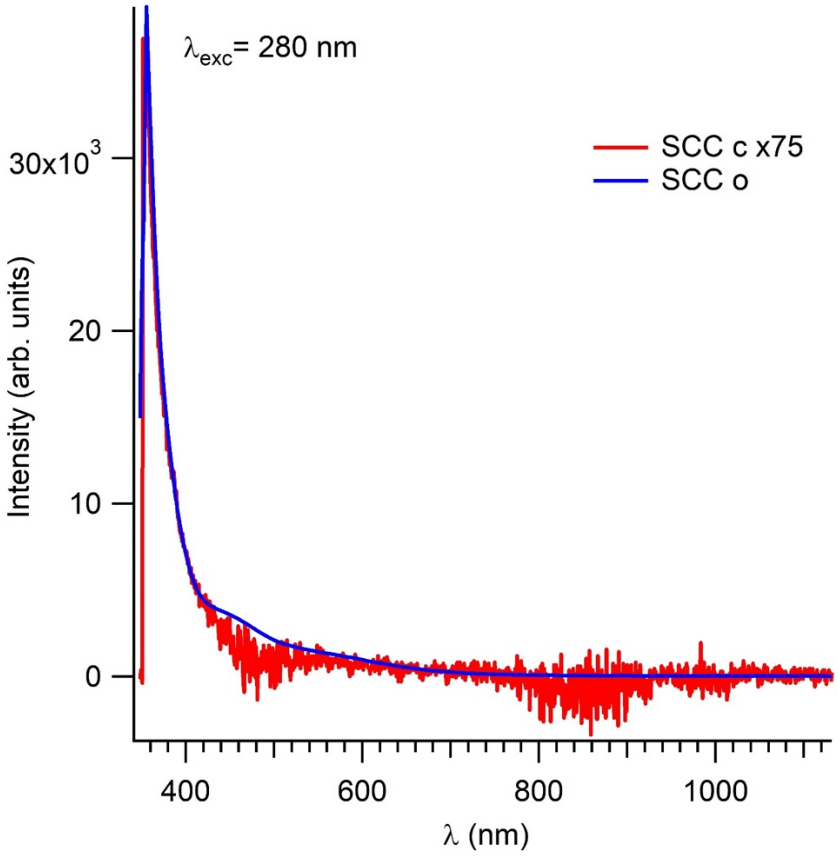
λexc= 280 nm
SCC c x75
SCC o
30x10^3
20
10
0
Intensity (arb. units)
400
600
800
1000
λ (nm)

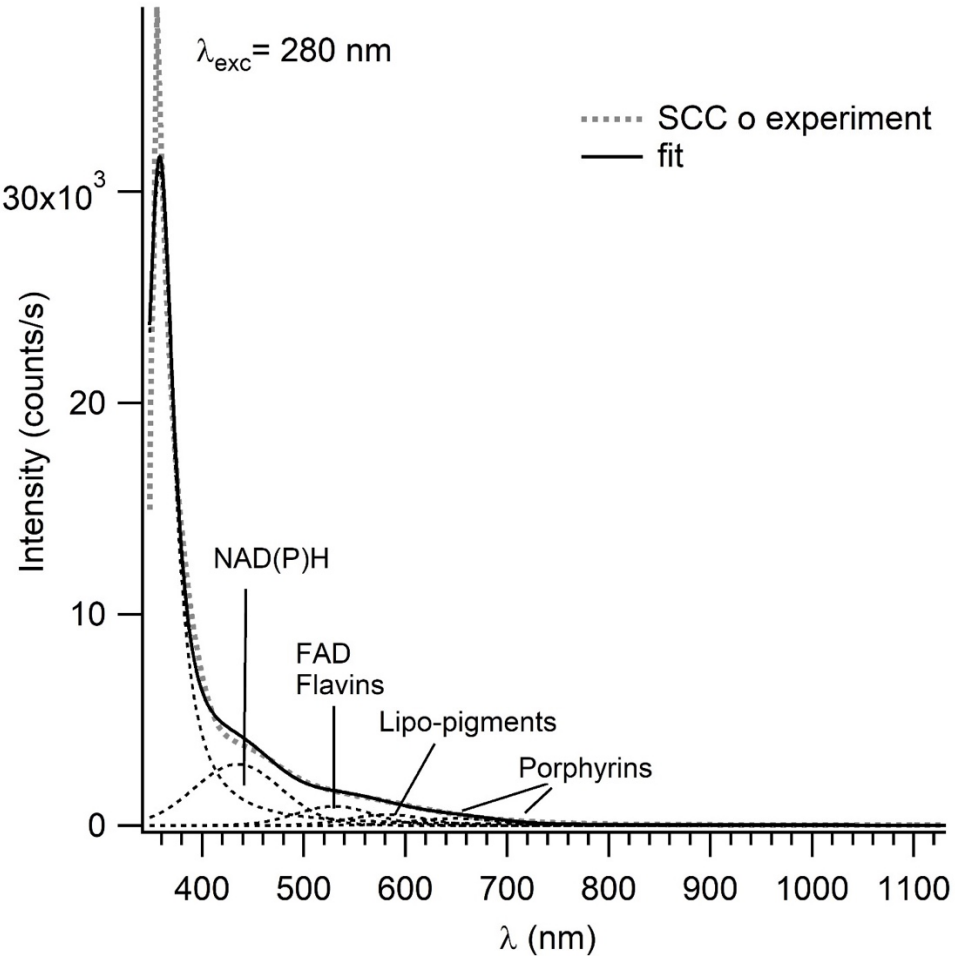
λexc= 280 nm
SCC o experiment
fit
30x10^3
20
10
0
Intensity (counts/s)
NAD(P)H
FAD
Flavins
Lipo-pigments
Porphyrins
400
500
600
700
800
900
1000
1100
λ (nm)

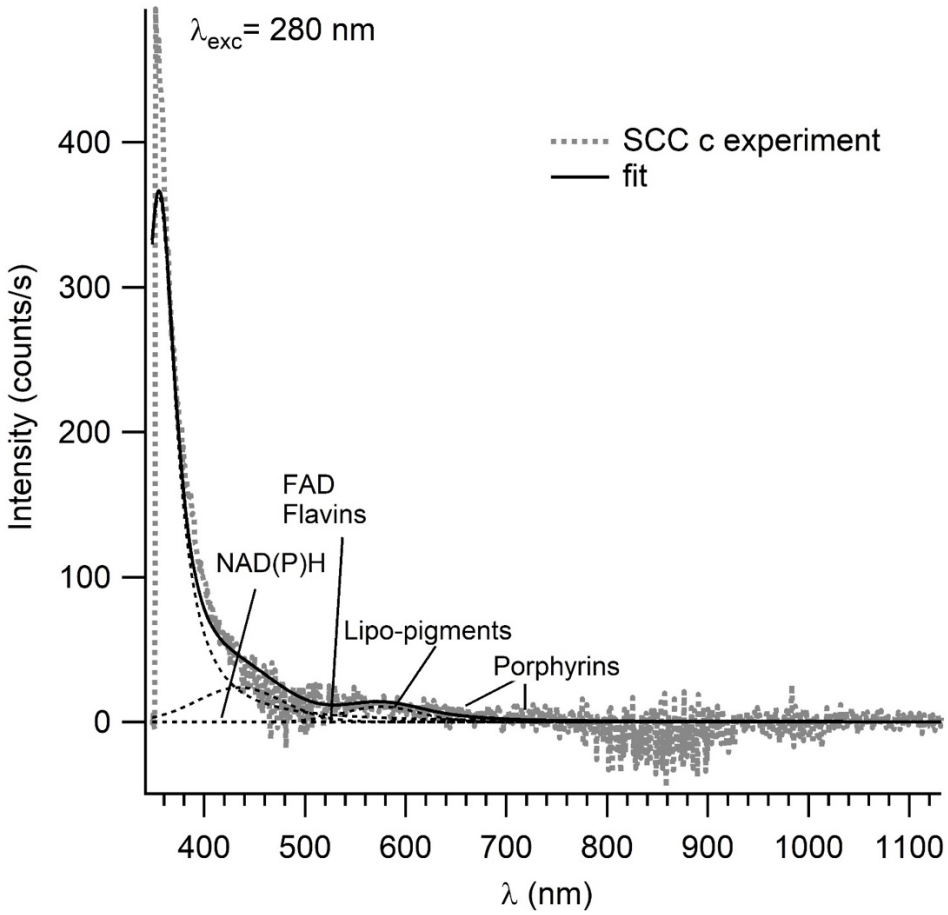

Figure 24: The fluorescence spectrum taken with λ_{exc} = 280nm is shown, together with a best-fit decomposition of features using Gaussian profiles of both oral SCC (o) and Skin SCC (c)

The second comparison involved the examination of SCC from the tongue and the skin, (Figure 23) with all cells originating from cell lines. Both demonstrated comparable characteristics, representing cells from tumors in a stratified, keratinized epithelium one from the oral mucosa and the other from the skin. The oral SCC line was HPV-positive and p53-negative, while, conversely, skin SCC was HPV-negative and had a mutated p53.

As demonstrated earlier, oral SCC displayed a hyperfluorescent appearance compared to skin SCC across all excitation wavelengths, with this distinction being

more pronounced in the lower excitation wavelengths. To gain further insights, we conducted a fitting process to extract additional information.

A notable observation, from the qualitative standpoint, assessable by fitting process, (Figure 24) was the weak FAD contribution in the fit of skin SCC in the third area, marking the initial divergence in terms of fluorophore contributions. Another crucial point to consider was the impact of intrinsic characteristics of the cell lines. Specifically, the skin tumor cell line exhibited a mutation in the p53 gene.

As we know, the deactivation of the p53 tumor suppressor is a common occurrence in tumorigenesis. Typically, the p53 gene undergoes mutations, resulting in the formation of a stable mutant protein. The accumulation of this mutant protein is considered a distinctive feature of cancer cells. Mutant p53 proteins not only forfeit their tumor-suppressive capabilities but frequently acquire extra oncogenic functions, providing cells with advantages in terms of growth and survival.

Moriichi et al.[72] demonstrated that p53 mutation in colon cancer determined a decrease of AF intensity compared to similar tumors without such mutation.

In line with these data, the absence of p53 mutation might have possibly played a role in the hyperfluorescent aspect of the SCC came from oral cavity instead skin SCC.

6 General Conclusions

This thesis, composed of a collection of studies conducted over three years, summarizes the results obtained through the study of autofluorescence in the setting of NMSC. Initially, we evaluated luminescence at a tissue level, on surgical specimens, to understand if there were discernible differences that could help us in distinguishing healthy skin from tumoral tissue. To the best of our knowledge, our study is unique for the systematic analysis of the variation of AFIR in relation to a series of histological variables. Our results suggest that the analysis of fluorescence intensity could be a reliable tool for the non-invasive identification of NMSCs. Such tools might also find application for the definition of surgical margins.

This initial work drove us to investigate this phenomenon at a cellular level. We recorded autofluorescence values in cell cultured in vitro, allowing us to differentiate healthy skin cells from some forms of cutaneous epithelial tumors. Healthy keratinocytes clearly showed characteristic features associated with specific chromophores [FAD and NAD(P)H, lipo-pigments, porphyrins], severely attenuated and smeared out in pathological cells. This is particularly evident in the UV excitation spectrum. Due to the variability of the overall AF intensity signal in different replicas of the same type of sample, multivariate analysis was performed on a series of datasets obtained on different freshly prepared replicas of control and SCC cells samples. The multivariate classification models based on PLS-DA allowed us to distinguish the two different AF curves of healthy and pathological cells, independently of overall spectral intensity and excitation wavelength. Due to the relatively limited number of available samples, the best classification model was further tested by means of a permutation test, whose results were then verified by a one-tailed t test that confirmed its statistical significance ($p = 0.003$ for the prediction of the test set samples). The AF spectral region between 550 and 670 nm was selected as the more meaningful to separate the two cell populations. Indeed, this is the region

where contributions from FAD, lipo-pigments and porphyrins show up. These differences between healthy keratinocytes and SCC cells were confirmed either on cells obtained from skin biopsies and cell lines, suggesting such characteristics to be constitutive rather than induced by the peritumoral stroma. We believe that these findings could provide a further tool toward the application of AF in fast and non-invasive diagnosis of skin cancer.

Not only these early encouraging results lay the groundwork for further clinical applications, but also prompted us to begin new studies on melanocytes and melanoma cells, despite melanin representing a significant challenge for luminescence evaluation.

Bibliography

1. Stokes, G. (1852). On the change of refrangibility of light (Vol. 142). Lond: Philos Trans R Soc.
2. Valeur, B., & Berberan-Santos, M. (2011). A Brief History of Fluorescence and Phosphorescence before the Emergence of Quantum Theory. Journal of Chemical Education, 88(6), 731-738.
3. Becquerel, E. (1867). La Lumière. Ses Causes et ses Effets. Paris: Firmin Didot.
4. Lakowicz, J. (1999). Principles Of Fluorescence Spectroscopy. New York: Kluwer Academic/Plenum.
5. Clarke, E. (1819). Account of a newly discovered variety of green flour spar, of very uncommon beauty and with remarkable properties of colour and phosphorescence.
6. Brewster, D. (1834). On the colours of natural bodies.
7. Díaz-García, M., & Badía-Laíño, R. (2019). Encyclopedia of Analytical Science (Third Edition). Spain: Paul Worsfold, Colin Poole, Alan Townshend, Manuel Miró.
8. Miyamoto, K., & Kudoh, H. (2013). Quantification and visualization of cellular NAD(P)H in young and aged female facial skin with in vivo two-photon tomography. British Journal of Dermatology, 169(Suppl 2), 25-31.
9. Croce, A., & Bottiroli, G. (2014). Autofluorescence spectroscopy and imaging: a tool for biomedical research and diagnosis. European Journal of Histochemistry, 58(4), 2461.
10. Gào, X., & Schöttker, B. (2017). Reduction–oxidation pathways involved in cancer development: a systematic review of literature reviews. Oncotarget, 8(31), 51888– 51906.
11. Drakaki, E.A., Dessinioti, C., Stratigos, A.J., Salavastru, C., and Antoniou, C. (2014). Laser-induced fluorescence made simple: implications for the diagnosis and follow-up monitoring of basal cell carcinoma. https://doi.org/10.1117/1.JBO.19.3.030901 19, 030901. 10.1117/1.JBO.19.3.030901.
12. Jayanthi, J.L., Mallia, R.J., Shiny, S.T., Baiju, K. V., Mathews, A., Kumar, R., Sebastian, P., Madhavan, J., Aparna, G.N., and Subhash, N. (2009). Discriminant analysis of autofluorescence spectra for classification of oral lesions in vivo. Lasers in Surgery and Medicine 41, 345–352. 10.1002/LSM.20771.
13. Drakaki, E., Vergou, T., Dessinioti, C., Stratigos, A. J., Salavastru, C., & Antonioua, C. (2013). Spectroscopic methods for the photodiagnosis of nonmelanoma skin cancer. Journal of Biomedical Optics.
14. Hoffmann, K., Stucker, M., Altmeyer, P., Teuchner, K., & Leupold, D. (2001). Selective femtosecond pulseexcitation of melanin fluorescence in tissue. Journal of Inves- tigative Dermatology, 116, 629–630.
15. Keyvan Nouri et. Al (2023) Skin Cancer: A Comprehensive Guide ISBN-10: 1260453006.
16. Correia de Sá, T.R., Silva, R., and Lopes, J.M. (2015). Basal cell carcinoma of the skin (part 1): epidemiology, pathology and genetic syndromes. Future Oncol *11*, 3011–3021. 10.2217/fon.15.246.
17. Boi, S., Cristofolini, M., Micciolo, R., Polla, E., and Palma, P.D. (2003). Epidemiology of Skin Tumors: Data from the Cutaneous Cancer Registry in Trentino, Italy. J Cutan Med Surg *7*, 300–305. 10.1007/s10227-002-0135-0.
18. Holmes, J., von Braunmühl, T., Berking, C., Sattler, E., Ulrich, M., Reinhold, U., Kurzen, H., Dirschka, T., Kellner, C., Schuh, S., et al. (2018). Optical coherence tomography of basal cell carcinoma: influence of location, subtype, observer variability and image quality on diagnostic performance. British Journal of Dermatology *178*, 1102–1110. 10.1111/bjd.16154.
19. Que, S.K.T., Zwald, F.O., and Schmults, C.D. (2018). Cutaneous squamous cell carcinoma. Journal of the American Academy of Dermatology *78*, 237–247. 10.1016/j.jaad.2017.08.059.
20. Karia, P.S., Han, J., and Schmults, C.D. (2013). Cutaneous squamous cell carcinoma: Estimated incidence of disease, nodal metastasis, and deaths from disease in the United States, 2012. Journal of the American Academy of Dermatology *68*, 957–966. 10.1016/j.jaad.2012.11.037.

21. Brancaccio, G., Napolitano, S., Troiani, T., Franco, R., Iovino, F., Reginelli, A., Ciardiello, F., and Argenziano, G. (2018). Eighth American Joint Committee on Cancer (AJCC) melanoma classification: what about stage IIC? British Journal of Dermatology. 10.1111/bjd.17145.
22. on behalf of the Italian Group of Dermato-Oncology (GIDO) of SIDeMaST, Peris, K., Alaibac, M., Argenziano, G., Di Stefani, A., Fargnoli, M.C., Frascione, P., Gualdi, G., Longo, C., Moscarella, E., et al. (2018). Cutaneous squamous cell carcinoma. Italian Guidelines by SIDeMaST adapted to and updating EADO/EDF/EORTC guidelines. G Ital Dermatol Venereol *153*. 10.23736/S0392-0488.18.06093-5.
23. Fahradyan, A., Howell, A.C., Wolfswinkel, E.M., Tsuha, M., Sheth, P., and Wong, A.K. (2017). Updates on the Management of Non-Melanoma Skin Cancer (NMSC). Healthcare *5*, 82. 10.3390/healthcare5040082.
24. Golda N, Hruza G. Mohs Micrographic Surgery. Dermatol Clin. 2023 Jan;41(1):39-47. doi: 10.1016/j.det.2022.07.006. Epub 2022 Oct 28. PMID: 36410982.
25. Lai, V., Cranwell, W., & Sinclair, R. (2018). Epidemiology of skin cancer in the mature patient. Clinics in Dermatology, 167–176.
26. Lomas, A., Leonardi-Bee, J., and Bath-Hextall, F. (2012). A systematic review of worldwide incidence of nonmelanoma skin cancer. British Journal of Dermatology *166*, 1069–1080. 10.1111/j.1365-2133.2012.10830.x.
27. Samarasinghe, V., & Madan, V. (2012). Nonmelanoma skin cancer. Journal of cutaneous and aesthetic surgery, 5(1), 3-10.
28. Kim, D.P., Kus, K.J.B., and Ruiz, E. (2019). Basal Cell Carcinoma Review. Hematology/Oncology Clinics of North America *33*, 13–24. 10.1016/j.hoc.2018.09.004.
29. Migden, M.R., Chang, A.L.S., Dirix, L., Stratigos, A.J., and Lear, J.T. (2018). Emerging trends in the treatment of advanced basal cell carcinoma. Cancer Treatment Reviews *64*, 1–10. 10.1016/j.ctrv.2017.12.009.
30. Marzuka, A. G., & Book, S. E. (2015). Basal Cell Carcinoma: Pathogenesis, Epidemiology, Clinical Features, Diagnosis, Histopathology, and Management. YALE JOURNAL OF BIOLOGY AND MEDICINE, 167-179.
31. McCusker, M., Basset-Seguin, N., Dummer, R., Lewis, K., Schadendorf, D., Sekulic, A., Hou, J., Wang, L., Yue, H., and Hauschild, A. (2014). Metastatic basal cell carcinoma: Prognosis dependent on anatomic site and spread of disease. European Journal of Cancer *50*, 774–783. 10.1016/j.ejca.2013.12.013.
32. Tagliaferri, L., Ciardo, F.G., Fionda, B., Casà, C., DI Stefani, A., Lancellotta, V., Placidi, E., Macchia, G., Capocchiano, N.D., Morganti, A.G., et al. (2021). Non-melanoma Skin Cancer Treated by Contact High-dose-rate Radiotherapy (Brachytherapy): A Mono-institutional Series and Literature Review. In Vivo *35*, 2313–2319. 10.21873/invivo.12505.
33. Peris, K., Alaibac, M., Argenziano, G., Di Stefani, A., Fargnoli, M., Frascione, P., Calzavara Pinton, P. (2018, Jun). Cutaneous Squamous Cell Carcinoma - Italian Guidelines by SIDeMaST adapted to and updating EADO/EDF/EORTC guidelines. Giornale Italiano di Dermatologia e Venereologia.
34. Dessinioti, C., Antoniou, C., & AJ, S. (2011). New targeted approaches for the treatment and prevention of nonmelanoma skin cancer. Expert review dermatology, 6(6), 625-634.
35. Seidenari, S., Arginelli, F., Bassoli, S., Cautela, J., French, P.M.W., Guanti, M., Guardoli, D., König, K., Talbot, C., and Dunsby, C. (2012). Multiphoton Laser Microscopy and Fluorescence Lifetime Imaging for the Evaluation of the Skin. Dermatology Research and Practice *2012*, 1–8. 10.1155/2012/810749.
36. Lupu, M., Voiculescu, V.M., Caruntu, A., Tebeica, T., and Caruntu, C. (2021). Preoperative Evaluation through Dermoscopy and Reflectance Confocal Microscopy of the Lateral Excision Margins for Primary Basal Cell Carcinoma. Diagnostics (Basel) *11*. 10.3390/diagnostics11010120.
37. Navarrete-Dechent, C., Cordova, M., Aleissa, S., Liopyris, K., Dusza, S.W., Kose, K., Busam, K.J., Hollman, T., Lezcano, C., Pulitzer, M., et al. (2019). Lentigo maligna melanoma

mapping using reflectance confocal microscopy correlates with staged excision: A prospective study. Journal of the American Academy of Dermatology, S0190962219331500. 10.1016/j.jaad.2019.11.058.
38. de Carvalho, N., Farnetani, F., Ciardo, S., Ruini, C., Witkowski, A.M., Longo, C., Argenziano, G., and Pellacani, G. (2015). Reflectance confocal microscopy correlates of dermoscopic patterns of facial lesions help to discriminate lentigo maligna from pigmented nonmelanocytic macules. Br J Dermatol *173*, 128–133. 10.1111/bjd.13546.
39. Reiter, O., Mimouni, I., Gdalevich, M., Marghoob, A.A., Levi, A., Hodak, E., and Leshem, Y.A. (2019). The diagnostic accuracy of dermoscopy for basal cell carcinoma: A systematic review and meta-analysis. Journal of the American Academy of Dermatology *80*, 1380–1388. 10.1016/j.jaad.2018.12.026.
40. Monici, M. (2005). Cell and tissue autofluorescence research and diagnostic applications. Biotechnology Annual Review, 11, 227-56.
41. Photodiagnosis for cutaneous malignancy: A brief clinical and technical review.
42. Meleti, M., Giovannacci, I., Vescovi, P., Pedrazzi, G., Govoni, P., & Magnoni, C. (2020). Histopathological determinants of autofluorescence patterns in oral carcinoma. Oral Disease, 10.1111/odi.13304. Advance online publication. .
43. Sandby-Møller, J., Thieden, E., Philipsen, P., Heydenreich, J., & Wulf, H. (2004). Skin autofluorescence as a biological UVR dosimeter. Photodermatology, Photoimmunology & Photomedicine, 20(1), 33-40.
44. Paolino, G., Donati, M., Didona, D., Mercuri, S., & Cantisani, C. (2017, Dec 20). Histology of Non-Melanoma Skin Cancers: An Update. Biomedicines, 5(71).
45. Nagi, R., Reddy-Kantharaj, Y.-B., Rakesh, N., Janardhan-Reddy, S., and Sahu, S. (2016). Efficacy of light based detection systems for early detection of oral cancer and oral potentially malignant disorders: Systematic review. Med Oral Patol Oral Cir Bucal *21*, e447-455. 10.4317/medoral.21104.
46. Lane, P., Gilhuly, T., Whitehead, P., Zeng, H., Poh, C., Ng, S., & al., e. (2006). Simple device for the direct visualization of oral-cavity tissue fluorescence. Journal of Bi- omedical Opticst, 11(2), 024006.
47. Monici, M. (2005). Cell and tissue autofluorescence research and diagnostic applications. Biotechnology Annual Review 11, 227–256. 10.1016/S1387-2656(05)11007-2.
48. Chang, S.K.; Follen, M.; Malpica, A.; Utzinger, U.; Staerkel, G.; Cox, D.; Atkinson, E.N.; MacAulay, C.; Richards-Kortum, R. Optimal excitation wavelengths for discrimination of cervical neoplasia. IEEE Trans. Biomed. Eng. 2002, 49, 1102–1111.
49. Zeng, H., MacAulay, C., McLean, D., & Palcic, B. (1995). Spectroscopic and microscopic characteristics of human skin autofluorescence emission. Photochemistry and Photobiology, 61, 39–645.
50. Borisova, E., Pavlova, P., Pavlova, E., Troyanova, P., and Avramov, L. (2012). Optical Biopsy of Human Skin-A Tool for Cutaneous Tumours' Diagnosis. INT. J. BIOAUTOMATION 16, 53–72.
51. He, Q.; Lui, H.; Zloty, D.; Cowan, B.;Warshawski, L.; McLean, D.I.; Zeng, H. Microscopic fluorescence spectral analysis of basal cell carcinomas. In Proceedings of the Fifth International Conference on Photonics and Imaging in Biology and Medicine, Wuhan, China, 1–3 September 2007; pp. 653414–653415.
52. Panjehpour, M., Julius, C., Phan, M., Vo-Dinh, T., & & Overholt, S. (2002). Laser-induced fluorescence spectroscopy for in vivo diagnosis of non-melanoma skin cancers. Lasers in surgery and medicine, 31(5), 367–373.
53. Brancaleon, L., Durkin, A., Tu, J., Menaker, G., Fallon, J., & & Kollias, N. (2001). In vivo fluorescence spectroscopy of nonmelanoma skin cancer.
54. Giovannacci, I., Magnoni, C., Vescovi, P., Painelli, A., Tarentini, E., & Meleti, M. (2019). Which are the main fluorophores in skin and oral mucosa? A review with emphasis on clinical

applications of tissue autofluorescence. Archivies of Oral Biology, 105, 89-98.
55. Bliznakova, I., Borisova, E., and Avramov, L. (2007). Laser- and Light-Induced Autofluorescence Spectroscopy of Human Skin in Dependence on Excitation Wavelengths. Acta Phys. Pol. A *112*, 1131–1136. 10.12693/APhysPolA.112.1131.
56. Navarrete-Dechent C, Pietkiewicz P, Dusza SW, Andreani S, Nehal KS, Rossi AM, Cordova M, Lee EH, Chen CJ, Abarzua-Araya A, Uribe P, Castro JC, Droppelmann K, Cardenas C, Marghoob AA. Ultraviolet-induced fluorescent dermoscopy for biopsy site identification prior to dermatologic surgery: A retrospective study. J Am Acad Dermatol. 2023 Oct;89(4):841-843. doi: 10.1016/j.jaad.2023.05.089. Epub 2023 Jun 15. PMID: 37328004.
57. Ramanujam, N., Mitchell, M.F., Mahadevan-Jansen, A., Thomson, S.L., Staerkel, G., Malpica, A., Wright, T., Atkinson, N., and Richards-Kortum, R. (1996). Cervical Precancer Detection Using a Multivariate Statistical Algorithm Based on Laser-Induced Fluorescence Spectra at Multiple Excitation Wavelengths. Photochemistry and Photobiology *64*, 720–735. 10.1111/j.1751-1097.1996.tb03130.x.
58. Sterenborg, H.J.C.M., Motamedi, M., Wagner, R.F., Duvic, M., Thomsen, S., and Jacques, S.L. (1994). In vivo fluorescence spectroscopy and imaging of human skin tumours. Lasers in Medical Science 1994 9:3 9, 191–201. 10.1007/BF02590223.
59. Franco, W., Gutierrez-Herrera, E., Kollias, N., and Doukas, A. (2016). Review of applications of fluorescence excitation spectroscopy to dermatology. British Journal of Dermatology 174, 499–504. 10.1111/BJD.14221.
60. Giovannacci, I., Meleti, M., Garbarino, F., Cesinaro, A.M., Mataca, E., Pedrazzi, G., Reggiani, C., Paganelli, A., Truzzi, A., Elia, F., et al. (2021). Correlation between Autofluorescence Intensity and Histopathological Features in Non-Melanoma Skin Cancer: An Ex Vivo Study. Cancers 2021, Vol. 13, Page 3974 13, 3974. 10.3390/CANCERS13163974.
61. Chernomyrdin, N. V., Lesnichaya, A. D., Yakovlev, E. V., Kudrin, K. G., Cherkasova, O. P., Rimskaya, E. N., . . . Zaytsev, K. I. (2019). Differentiation of basal cell carcinoma and healthy skin using multispectral modulation autofluorescence imaging: A pilot study.
62. Meena, B.L., Agarwal, A., Pantola, C., Pandey, K., and Pradhan, A. (2019). Concentration of FAD as a marker for cervical precancer detection. https://doi.org/10.1117/1.JBO.24.3.035008 24, 035008. 10.1117/1.JBO.24.3.035008.
63. Croce, A., Santamaria, G., De Simone, U., Lucchini, F., Freitas, I., & Bottiroli, G. (2011). Naturally-occurring porphyrins in a spontaneous-tumour bearing mouse model. Photochemical & Photobiological Sciences, 10(7), 1189-95.
64. Drakaki, E., Dessinioti, C., Stratigos, A., Salavastru, C., & Antoniou, C. (2014). Laser-induced fluorescence made simple: implications for the diagnosis and follow-up monitoring of basal cell carcinoma. Journal of Biomedical Optics, 19(3), 30901.
65. Skala, M., Riching, K., Bird, D., Fitzpatrick, A., Eickhoff, J., Eliceiri, K., Ramanujam, N. (2007). In vivo multiphoton fluorescence lifetime imaging of protein-bound and free nicotinamide adenine dinucleotide in normal and precancerous epithelia. Journal of Biomedical Opticst, 12, 024014.
66. Johnson, T.M., Hielscher, A.H., Eick, A.A., Mourant, J.R., Freyer, J.P., and Shen, D. (1998). Mechanisms of light scattering from biological cells relevant to noninvasive optical-tissue diagnostics. Applied Optics, Vol. 37, Issue 16, pp. 3586-3593 37, 3586–3593. 10.1364/AO.37.003586.
67. Pigani, L., Culetu, A., Ulrici, A., Foca, G., Vignali, M., and Seeber, R. (2011). Pedot modified electrodes in amperometric sensing for analysis of red wine samples. Food Chemistry 129, 226–233. 10.1016/J.FOODCHEM.2011.04.046.
68. Garbarino F, Scelfo D, Paulone G, Paganelli A, Ulrici A, Magnoni C, Pasquali L. Comparative study of in-vitro autofluorescence of normal versus non-melanoma-skin-cancer cells at different excitation wavelengths. J Biophotonics. 2023 May;16(5):e202200361. doi: 10.1002/jbio.202200361. Epub 2023 Jan 25. PMID: 36645389.

69. Drakaki, E., Dessinioti, C., Stratigos, A.J., Salavastru, C., and Antoniou, C. (2014). Laser-induced fluorescence made simple: implications for the diagnosis and follow-up monitoring of basal cell carcinoma. J. Biomed. Opt *19*, 030901. 10.1117/1.JBO.19.3.030901.
70. Wolman M. Lipid pigments (chromolipids): their origin, nature and significance. Pathobiol Ann 1980;10:253-67.
71. Santin G, Paulis M, Vezzoni P, Pacchiana G, Bottiroli G, Croce AC. Autofluorescence properties of murine embryonic stem cells during spontaneous differentiation phases. Lasers Surg Med 2013 Nov;45:597-607.
72. Moriichi K, Fujiya M, Kobayashi Y, et al. Autofluorescence Imaging Reflects the Nuclear Enlargement of Tumor Cells as well as the Cell Proliferation Ability and Aberrant Status of the p53, Ki-67, and p16 Genes in Colon Neoplasms. Molecules. 2019;24(6):1106. Published 2019 Mar 20. doi:10.3390/molecules24061106.